

Surface-modified gelatin hydrogel scaffolds with imprinted microgrooves: physical characterization and study on endothelial cell interaction

Ali Salehi, Lena Rutz, Konstantin Ulbrich, Johanna Stevens, Markus Guttman, Matthias Worgull & Giorgio Cattaneo

To cite this article: Ali Salehi, Lena Rutz, Konstantin Ulbrich, Johanna Stevens, Markus Guttman, Matthias Worgull & Giorgio Cattaneo (20 Jul 2025): Surface-modified gelatin hydrogel scaffolds with imprinted microgrooves: physical characterization and study on endothelial cell interaction, Journal of Biomaterials Science, Polymer Edition, DOI: [10.1080/09205063.2025.2527912](https://doi.org/10.1080/09205063.2025.2527912)

To link to this article: <https://doi.org/10.1080/09205063.2025.2527912>



© 2025 The Author(s). Published by Informa UK Limited, trading as Taylor & Francis Group



[View supplementary material](#)



Published online: 20 Jul 2025.



[Submit your article to this journal](#)



Article views: 112








[View related articles](#)



[View Crossmark data](#)

Surface-modified gelatin hydrogel scaffolds with imprinted microgrooves: physical characterization and study on endothelial cell interaction

Ali Salehi^a , Lena Rutz^a , Konstantin Ulbrich^a, Johanna Stevens^a , Markus Guttman^b , Matthias Worgull^b and Giorgio Cattaneo^a 

^aInstitute of Biomedical Engineering, University of Stuttgart, Stuttgart, Germany; ^bInstitute of Microstructure Technology (IMT) and Karlsruhe Nano Micro Facility (KNMFi), Karlsruhe Institute of Technology (KIT), Karlsruhe, Germany

ABSTRACT

Endothelialization of biomaterials enhances biocompatibility, hemocompatibility, and reduces inflammatory responses in blood-contacting materials. Surface topographies, particularly groove-like structures, influence endothelial cell morphology and function. This study investigates the impact of microgroove dimensions on endothelialization in gelatin hydrogel scaffolds, alongside assessing their physical and mechanical properties. Using sequential replications, six microgroove geometries with widths ranging from 2.86 μm to 84.20 μm and depths from 284 nm to 919 nm were fabricated on gelatin hydrogel. Surface characterization of the scaffolds over 5 days using confocal microscopy revealed a shrinkage followed by dimensional stability after 24 h. Tensile testing after conditioning in cell culture environments showed Young's modulus of 327.2–529.5 kPa comparable to natural blood vessels. Cultivation of human endothelial cells demonstrated improved cell orientation and elongation on microstructured surfaces. Notably, two specific microgrooved scaffolds (9.33 μm width, 599 nm depth and 22.27 μm width, 919 nm depth) enhanced cell proliferation, adhesion and accelerated confluent monolayer formation as confirmed through fluorescent staining for cell nuclei, Vinculin, and VE-cadherin expression, respectively. This study identifies optimal microgroove dimensions for surface modification of gelatin hydrogel scaffolds demonstrating how geometric cues can positively impact cell morphology and function. This surface engineering approach has a potential application in *in vitro* endothelialized models for cardiovascular research as well as in vascular implants for tissue remodeling.

ARTICLE HISTORY

Received 11 April 2025

Accepted 26 June 2025


KEYWORDS

Surface engineering; endothelialization; microgrooves; surface characterization; HUVECs; hydrogel scaffold

1. Introduction

Cardiovascular diseases (CVD), including coronary artery disease and stroke, represent the leading cause of mortality worldwide [1]. To address the increasing

CONTACT Ali Salehi ✉ ali.salehi@bmt.uni-stuttgart.de  Institute of Biomedical Engineering, University of Stuttgart, Stuttgart, Germany

 Supplemental data for this article can be accessed online at <https://doi.org/10.1080/09205063.2025.2527912>.

© 2025 The Author(s). Published by Informa UK Limited, trading as Taylor & Francis Group

This is an Open Access article distributed under the terms of the Creative Commons Attribution License (<http://creativecommons.org/licenses/by/4.0/>), which permits unrestricted use, distribution, and reproduction in any medium, provided the original work is properly cited. The terms on which this article has been published allow the posting of the Accepted Manuscript in a repository by the author(s) or with their consent.

prevalence of CVD, there is a growing need for advancements in intravascular implants, tissue-engineered vascular grafts, as well as vessel models for their *in vitro* investigation. Among the biomaterials used to produce vessel-mimicking tubular structures, hydrogels offer biocompatibility and tunable physical and mechanical properties making them a suitable choice for vascular tissue engineering applications. Vascular hydrogel vessel models made of acrylamide and polyvinyl alcohol, which mimic the physical and mechanical properties of natural blood vessels, have been used as models for surgical hemostasis training [2]. Synthetic hydrogels, such as poly(ethylene glycol) (PEG), poly(lactic-co-glycolic acid) (PLGA), and poly(glycerol sebacate) (PGS)-based hydrogels, have been employed to fabricate complex prevascularized networks with embedded cells for *in vitro* studies on angiogenesis and vascular function [3–5]. Due to their enhanced cell adhesion properties, tunable mechanical properties, shapeability, and low immunogenicity, gelatin-based hydrogels have gained particular attention [6].

Endothelium, a monolayer of endothelial cells lining the inner surface of blood vessels that plays a vital role in hemostasis and vascular tone regulation, is strongly associated with the pathophysiology of atherosclerosis [7]. In biomaterials for vascular engineering, endothelialization refers to the building of a healthy and functional layer of endothelial cells on the biomaterial surface. Contact guidance is the phenomenon wherein physical cues in a cell's surrounding microenvironment are converted into biochemical and intracellular responses through mechanotransduction, ultimately altering cellular function [8]. This mechanobiological effect governs cell proteins synthesis, morphology, adhesion, proliferation, differentiation, and migration [9,10]. The microenvironment of cells *in vivo*, defined as extracellular matrix (ECM), provides three-dimensional (3D) physical cues, including micro and nanoscale topographies [11,12]. Engineered surfaces with various micro- and nanoscale structures, including grooves, pillars, pits, wrinkles, and fibrous scaffolds, have been developed on different biomaterial surfaces including hydrogels, synthetic and natural polymers, and metals to create an optimized environment conducive to cellular organization and functionality [13,14]. Among different surface topographies, nano and micro-scale grooves are one of the most common surface topographies that enhance cell attachment, proliferation, and guide the migration of endothelial cells [15,16]. These grooves are typically fabricated with repeating patterns of uniform ridge widths and defined depths, which are tailored for different cell types such as fibroblasts, epithelial cells, and endothelial cells [17]. Groove widths, which are on the same order of magnitude as cell size, influence the overall cell morphology and cytoskeleton organization, thereby supporting the regulation of proliferation, migration, and immune responses by providing geometrical guidance [17–19]. Groove dimensions in the nanometer range are designed to mimic the architecture of the nanofibers in ECM. These features, being smaller than individual cells, enhance cell anchorage, alignment and interactions at the molecular level which can promote cellular behavior like adhesion and differentiation [17,20,21]. Moreover, cellular integrins, key components of the focal adhesion complex, exhibit a higher affinity for bonding to nanoscale microenvironments in comparison to smooth substrates [22]. Therefore, in designing surface topographies, it is crucial to consider both the nano- and micro-scale features.

Understanding the interactions between cells and biomaterial surfaces can enhance our ability to engineer biomaterial surfaces strategically. Tissue engineering of vascular grafts focuses on promoting rapid endothelialization, thereby minimizing the risk of thrombosis and vascular restenosis. To promote rapid endothelialization, several functional enhancements, including the incorporation of topographical, biochemical, and mechanical features that mimic native vessel characteristics, have been integrated into the design and fabrication of the grafts [23]. It has been shown that endothelialization of biomedical devices enhances their antithrombotic and anti-stenotic properties. Additionally, rapid re-endothelialization of the biomaterial surface can reduce the reliance on anticoagulatory drugs by improving the anti-inflammatory environment [24]. Moreover, *in vitro* surface-engineered vessel models with a functional, confluent layer of endothelial cells prevent blood clot formation by maintaining an anticoagulant surface, thereby allowing for the integration of blood into the test system and thus providing more reliable results in thrombosis-related studies [25].

Replicating cellular elongation and alignment *in vitro* is crucial to reestablish a biological and mechanical microenvironment that closely resembles *in vivo* conditions, thereby ensuring the reliability and applicability of *in vitro* studies [26]. Elongation and alignment of endothelial cells have been identified as key physical factors that influence the expression of immunogenic genes and the overall function of endothelial cells, even in the absence of shear stress [27]. The integration of structural cues on biomaterials may promote attachment and further alignment of endothelial cells [28]. To achieve cellular elongation and alignment, various techniques have been employed, including surface chemical modifications using cell-adhesive or repellent patterns; mechanical stimulation through dynamic and periodic substrate stretching or compression; the application of fluid shear stress; and the incorporation of topographical features such as microgrooves or nanofibers [29]. Regarding endothelial cells, studies have been dominantly carried out on surfaces with linear grooved patterns created by molding, photolithography, micro-machining, electron beam lithography and laser etching. These modifications have been performed on polymers such as Polydimethylsiloxane (PDMS), polycaprolactone (PCL), and PLGA; and hydrogels including Agarose, Heparin, PEG, Hyaluronic acid, and gelatin [30,31]. Under physiological conditions, endothelial cells exposed to fluid shear stress reorganize their actin filaments and microtubules, aligning and elongating in the direction of blood flow. However, it is advantageous to develop methods for aligning endothelial cells *in vitro* without relying on shear stress, as this can simplify the experimental setup. Moreover, this has significant applications in the case of turbulence or flow stagnation due to the presence of intravascular devices or pathological conditions. Under such circumstances, endothelial cells exposed to turbulent flow often exhibit a non-aligned morphology [32]. Additionally, engineering biomaterial surfaces with topographical cues not only supports cell alignment but also promotes rapid endothelialization of biomaterials. This approach reduces the risk of thrombogenicity and enhances the long-term functionality of biomaterials in clinical applications.

An increasing number of studies have explored cellular behavior on microstructured surfaces made of materials such as metals, silicon rubber, and polydimethylsiloxane (PDMS) [33,34]. However, it is crucial to conduct similar investigations using biomaterials that possess comparable mechanical properties to native tissues.

Hydrogels, with their ability to mimic ECM microenvironment, are excellent choices as scaffolds for tissue engineering research. Among them, gelatin hydrogels have gained significant attention in biomedical engineering due to their biocompatibility, optical transparency, cost-effectiveness, and mechanical properties that closely resemble native tissues [35]. Gelatin, a product of collagen hydrolysis, is a key component of ECM and recognized as a biocompatible material [36]. The presence of glycine, proline, hydroxyproline, and Arginine–Glycine–Aspartic acid (RGD) sequences in gelatin hydrogels provides an ECM-like environment that supports cell adhesion, proliferation, nutrient exchange, and waste removal, making gelatin highly suitable for applications in tissue engineering and therapeutic delivery [37]. Transglutaminase is widely regarded as the most extensively studied enzyme for protein-based hydrogel cross-linking in tissue engineering applications [38]. It enables the precise crosslinking of proteins by forming conjugates at specific glutamine (Gln) and lysine (Lys) chains [39]. Microbial Transglutaminase (mTG) is approved by the Food and Drug Administration (FDA) and recognized for its cost-effectiveness [40], non-toxicity, and ability to enable the formation of permanent gelatin-based hydrogels [36]. Gelatin hydrogels crosslinked with transglutaminase have been reported to be mechanically stronger and more stable when compared to those crosslinked with other agents [41].

This study presents a novel approach by (1) introducing a straightforward micro-molding technique for generating microgroove patterns on gelatin hydrogels, (2) systematically investigating endothelialization using labelling markers which indicate cell-to-cell and cell-to-substrate anchoring across a wider range of microgroove dimensions on enzymatically crosslinked gelatin scaffolds, and (3) characterizing the physical, mechanical, and surface properties changes of the hydrogels before and during 14 days of incubation under physiological conditions in a cell culture environment. Previous studies generally introduced complex and time-consuming replication processes for structuring the surface of hydrogel scaffolds, such as 3D bioprinting [42] and electrospinning [43]. The enzymatic crosslinking method offers advantages over other gelatin hydrogel crosslinking techniques, including enhanced biocompatibility, the absence of residual crosslinker toxicity, and tunable mechanical properties. The grooves in this study, exhibit a width ranging from 3 to 100 micrometers (3, 5, 10, 25, 50, and 100 μm) and submicron depth, encompassing both nanoscale and microscale features. These dimensions mimic the topographical characteristics of vessel lumens and align with the dimensions reported in previous studies as beneficial for endothelialization [44]. Following mechanical and physical characterization of the gelatin hydrogel using tensile and swelling tests, we investigated the dimensional changes in surface structures during incubation in simulated cell culture conditions. The influence of surface cues was assessed by measuring the orientation angle and cell shape index, both of which are key parameters in describing contact guidance and morphological changes of cells on microgrooved substrates. Finally, we examined the influence of the six developed surface modifications on endothelialization. This included comparing cell proliferation, alignment, elongation, attachment strength, and endothelium formation. Fluorescent staining of cell nuclei and actin filaments was used, along with measurements of cell shape index and orientation angle, as well as vinculin and VE-cadherin expression, to evaluate these parameters.

2. Materials and methods

2.1. Hydrogel preparation and incubation

To better understand the behavior of gelatin hydrogels during extended storage time under physiological conditions, standardized samples were prepared, and their dimensions and weights were measured over 14 days. A gelatin solution suitable for enzymatic crosslinking was created as previously described [14,45]. In short, Type A gelatin from porcine skin (300 g bloom, Sigma-Aldrich, Germany) was completely dissolved in deionized water at 60 °C to make a 13 wt.% prepolymer solution. Microbial transglutaminase (mTG, specific activity of approximately 100 U/g, ACTIVIA® WM, Ajinomoto Foods Europe, France) was then added and thoroughly mixed with the gelatin solution to form a mixture with the final weight ratio of mTG to gelatin 1:10 (Figure 1). Immediately, the prepared solution was carefully transferred to cylindrical molds and kept overnight in the lab fridge at 4 °C. Cylindrical gelatin hydrogel samples ($n=6$) with a length of 5 mm and a diameter of 8 mm were fabricated. Two separate groups of sterile samples were designated for studying weight and dimensional changes. The samples were stored in an endothelial cell culture medium, with the medium refreshed every two days to simulate typical cell culture conditions and maintain pH within the cell culture range. This approach mimicked the environmental conditions experienced by hydrogels when used as endothelialized scaffolds. The samples were incubated at 37 °C, with 5% CO₂ and 80% humidity, to replicate the physiological environment. Each sample was individually weighed, and the diameter was measured using a stereomicroscope, with three measurements per specimen. Measurements were taken prior to incubation and on days 1, 2, 3, 4, 5, 7, and 14 after incubation. The changes in dimension and weight were calculated by $\nabla\% = \frac{x_{AI} - x_{PI}}{x_{PI}} \times 100$, where X is the weight or dimension of samples after incubation (AI) and prior to incubation (PI).

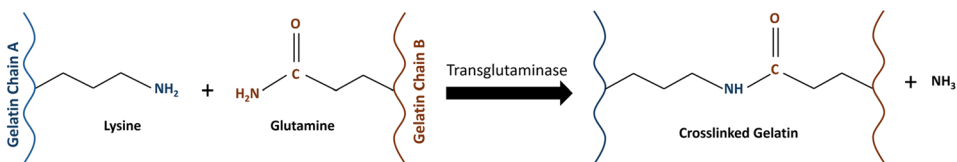


Figure 1. Enzymatic crosslinking of gelatin by microbial transglutaminase. The enzyme mTG catalyzes the formation of covalent bonds between the γ -carboxamide group of a glutamine residue on one gelatin chain and the ϵ -amino group of a lysine residue on another chain, yielding an ϵ -(γ -glutamyl)lysine isopeptide linkage and releasing ammonia.

2.2. Tensile test

To assess the mechanical properties of gelatin hydrogel prior and post-incubation in endothelial cell culture medium under the same condition as storage test, tensile testing was conducted on the samples before incubation and after incubation at days 1, 2, 3, 4, 5, 7 and 14 using a tensile machine (INSTRON 34SC-1, USA) with a 50 N load capacity. The test was performed on 5 samples ($n=5$) at a strain rate of 5 mm/

min and Young's modulus was calculated from the stress-strain curves as the slope of the linear region between 0.01% and 10% strain.

2.3. Production of microstructures on PMMA substrate

Parallel microgrooves with depths of 1 μm , and widths of 3, 5, 10, 25, 50, and 100 μm , with inter-groove distances matching their respective widths, were fabricated using laser lithography. Initially, 4-inch silicon wafers (thickness = 252 nm) were treated with Hexamethyldisilazane (HDMS) as an adhesion promoter at 140 $^{\circ}\text{C}$ in an oven (IMTEK, Star-2000, Germany). Following this, a 1 μm thick AZ1505 resist layer was applied by spin coating at 1000 rpm for 60 s, with a ramp rate of 1500 rpm/min (OPTicoat ST22+ Spin Coater, Robotechnik Europe, Germany). The coated wafers were then prebaked at 95 $^{\circ}\text{C}$ for 1 min on a hotplate. Subsequently, the substrates were exposed to a laser beam using a 4 mm write head at 30 mW laser power and 25% intensity (DWL 66+ Ultimate Lithography System, Heidelberg Instruments, Germany). The exposed resist patterns were then treated with a 25% AZ 400K (Merck Performance Materials, Germany) solution in water for 30 s using a spray developer (Optiwer St30, Robotechnik Europe, Germany). Finally, the patterned wafers were transferred into Nickel shims *via* electroplating and subsequently replicated onto 1 mm thick polymethyl methacrylate (PMMA) substrates by hot embossing at 165 $^{\circ}\text{C}$ and 35 kN (Hot embossing machine Jenoptik HEX03, Germany). The microgrooves, with each dimension, were diced to an area of 10 \times 10 mm² on the PMMA substrates and stored in a clean environment.

2.4. Microstructure replication on PDMS substrate

To achieve more microstructured negative substrates and enable the simultaneous fabrication of a sufficient number of microstructured hydrogel scaffolds, while preserving the integrity and quality of the PMMA substrates, the microstructures were initially replicated onto PDMS substrates. These PDMS substrates were then used to transfer the microstructures onto gelatin hydrogel scaffolds. For replicating the microstructures on Polydimethylsiloxane (PDMS) substrates, the PMMA substrate was placed on a 15 cm Petri dish with microstructures facing upward and fixed using autoclave tape. A 1:10 weight mixture of silicon elastomer curing agent and silicon elastomer base (DOWSIL 184, DOWTM, USA) was prepared and degassed at 0.8 bar for 10 min using a laboratory vacuum desiccator. Thirty grams of the mixture was gently poured into the Petri dish, ensuring it completely covered the surface of the PMMA substrate. The PDMS was poured into an empty Petri dish for the control group. The Petri dishes were then carefully placed in a laboratory oven at 70 $^{\circ}\text{C}$ for 2 h to allow for cross-linking. After reaching room temperature, the PDMS substrate was peeled off the PMMA gently. This process was repeated nine times to obtain nine PDMS replications from each structure dimension.

2.5. Preparation of microstructured hydrogel scaffolds

The surface engineering process for the preparation of microstructured scaffolds is illustrated in [Figure 2](#). After the crosslinking process, the 6 structured areas (3, 5,

10, 25, 50 and 100 μm) and one area with no structure as a control were cut into $8 \times 8 \text{ mm}^2$ squares, removed from the PDMS substrates and placed in a new Petri dish, structures facing upward. A mixture of gelatin solution with mTG was prepared as previously described and was immediately transferred to a Petri dish and kept overnight in the lab fridge at 4°C . Subsequently, the hydrogels from both the structured and control groups were detached from the PDMS and punched to fit the dimensions of 24-well plates, resulting in an $8 \times 8 \text{ mm}^2$ recessed structured or smooth area at the center of the surface-modified and control hydrogel scaffolds, respectively. For the control group on the tissue culture plate (TCP), a round PDMS substrate with an $8 \times 8 \text{ mm}^2$ open square area in the center was prepared and placed on the wells to ensure the same surface area of the well was accessible as on the surface-modified and control hydrogel scaffolds. The scaffolds underwent sterilization with 70% ethanol for 10 min and UV exposure for 30 min in a laminar flow hood, followed by a one-day incubation in cell culture media prior to cell seeding. To qualitatively assess successful replication and presence of microstructures on the hydrogel scaffolds before cell seeding, the scaffolds were imaged after a one-day incubation in cell culture medium (Endothelial Cell Growth Medium, Cat.No.C-22010, PromoCell, Germany) at a cell culture incubator using an inverted light microscope (Zeiss, Axio Vert.A1, Germany) at 20x magnification.

2.6. Surface characterization

The surface topography of the PMMA master substrate and the replication quality of the microstructures on three repeats of PDMS substrates and corresponding gelatin hydrogels were analyzed after production by measuring the dimensions of the microgrooves using confocal microscopy (MarSurf CM explorer, Nanofocus, Germany) and provided MarSurf MfM software. Microscopy of the hydrogels was performed immediately to minimize dehydration. To evaluate the effect of incubating gelatin hydrogel scaffolds in cell culture medium (Endothelial Cell Growth Medium, Cat. No. C-22010, PromoCell, Germany) under standard conditions (Cell culture incubator, 37°C , 5% CO_2) on microgroove dimensions—which may influence cell behavior during endothelialization—three samples ($n=3$) were incubated for 5 days and analyzed using the confocal microscopy on days 1, 3, and 5. The samples were kept hydrated using the same incubating cell culture medium solution and during microscopy, 6 random locations were selected on each of the three replicates of a sample. At each location, the height and width of two pairs of valleys and ridges were measured by the confocal microscope, resulting in a total of 36 values for both width and height measurements. A magnification of 100x was used for samples measuring 3, 5, and 10 μm , 50x for those measuring 25 and 50 μm , and 10x for the 100 μm sample.

2.7. Cell culture and seeding

Human Umbilical Vein Endothelial Cells (HUVEC) isolated in Growth Medium 2, pooled, (PromoCell, Germany) were cultured using the Endothelial Cell Growth Medium 2 Kit (PromoCell, Germany) until reaching 80% confluence. A cell

suspension of 1×10^5 cells/mL was prepared from HUVECs at passage number five. Then, 100 μ L of the cell suspension was seeded into the designated 8×8 mm² area of each well in a 24-well tissue culture plate, containing both non-structured and structured scaffolds pre-incubated for 1 day in cell culture medium, achieving a cell density of 1×10^4 cells per well. In the control group, cells were seeded on the same surface area and under optimal conditions on a 24-well tissue culture plate (TCP) with Nunclon Delta treatment, a surface treatment designed to maximize cell adhesion. After allowing the cells to adhere to the substrates for 5 h, 400 μ L of endothelial cell growth medium was added to each well. All seeded cells on the scaffolds and TCP were incubated in a cell culture incubator at 37°C with 5% CO₂ overnight for the first medium change. Thereafter, the medium was replaced every second day.

2.8. Cell staining and morphological analysis

Prior to fluorescent staining, a cell fixation process was performed by incubating the cells on the scaffolds and TCP in a 4% solution of Paraformaldehyde (Alfa Aesar, USA) in Phosphate-buffered saline (PBS, Sigma Aldrich, Germany) for 20 min followed by three washes with PBS on days 1, 2 and 3. To visualize the nuclei of the cells in each group, the fixed cells were stained with 4', 6-diamidino-2-phenylindole (DAPI) staining solution (Abcam, Germany). An F-actin staining Kit (Green Fluorescence, Cytopainter ab112125, Abcam, Germany) was used to observe the actin filaments of adhered cells on the substrates and assess the orientation angle of cells on the first day of endothelialization. The characteristic morphology of cells from all repetitions within each group was captured, visualizing Actin filaments and DAPI staining. On the last day of endothelialization, the cells were permeabilized with 0.01% Triton X-100 for 3 min and were blocked by 10% normal goat serum for 30 min before immunofluorescent staining. VE-cadherin, an exclusive marker of endothelial cells indicative for intra-cellular junctions was stained by a fluorescent-labeled anti-VE-cadherin antibody (Alexa Fluor® 647 conjugated, Santa Cruz Biotechnology, Inc., USA). Shape index and aspect ratio of cells were evaluated and representative images of each sample were captured *via* fluorescence microscopy. Furthermore, endothelial cell adhesion to the substrates was assessed by staining with a Vinculin antibody (Recombinant Alexa Fluor® 647 Anti-Vinculin, Abcam, Germany) to high-light focal adhesions.

All the fluorescent imaging was conducted using an inverted fluorescent microscope (ZEISS Axio Vert.A1, Carl Zeiss Suzhou Co., Ltd.) and ZEISS ZEN 3.7 software for image analysis. Cell proliferation was assessed by quantifying the number of cell nuclei using Bio Apps software (Zen Blue, Zeiss, Germany) in nine randomly selected images per group, covering the majority of the substrate's surface area. Vinculin expression within cells was analyzed by measuring fluorescence intensity. Regions of interest (ROI) within individual cells were selected, and the intensity of the red fluorescence channel was quantified using Zeiss image analysis software. This process was performed for each experimental condition, and the average Vinculin fluorescence intensity was calculated from 50 individual cells per group. Similarly, fluorescence intensity was measured to quantify VE-cadherin expression by creating 50 randomly selected ROIs fit to the cellular junctions in each group. To analyze the

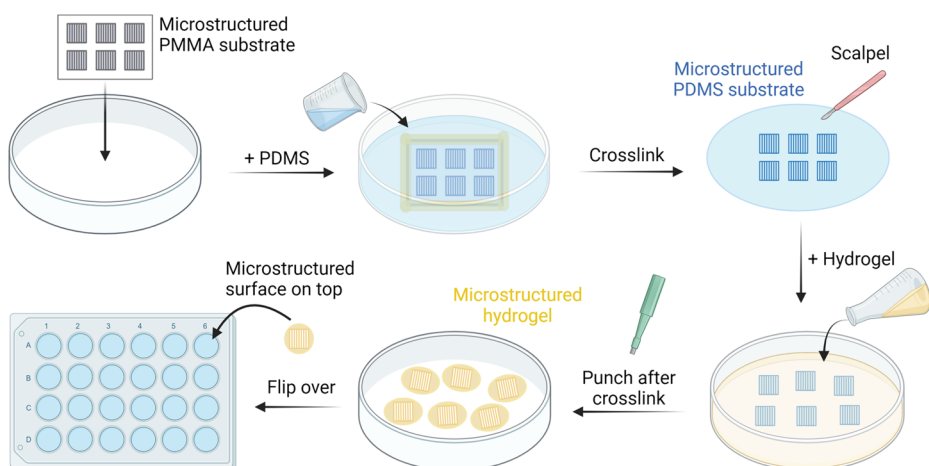


Figure 2. Schematic picture of surface engineering of gelatin hydrogel scaffolds by microgrooves created with BioRender.com.

impact of surface modification of scaffolds on the morphology of endothelial cells the following evaluations were performed. The shape index of 20 individual cells in different groups was obtained from the following equation by analyzing the fluorescent images using ImageJ software (version 1.8, NIH, USA). The shape index is one for a circle and zero for a line.

$$\text{shape index} = 4\pi \times \frac{\text{area}}{(\text{perimeter})^2}$$

The major and minor axes of the cells were identified and designated as the cells' length and width, respectively. The aspect ratio of 20 different cells was then calculated using the formula: Aspect Ratio = Length/Width. For a circular cell, the aspect ratio equals 1 and increases as the cell becomes more elongated. Furthermore, the orientation angle (θ) of the endothelial cells was determined by measuring the angle between the major axis of each cell ($n=20$) and the grooves' axis as depicted in Figure 3.

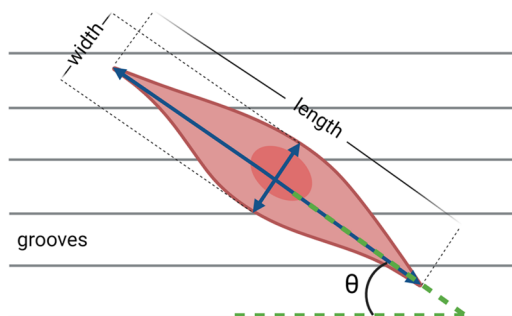


Figure 3. Schematic picture of a single endothelial cell on a microgrooved scaffold created with BioRender.com.

2.9. Statistics

In this study, all the experiments were repeated three times ($n=3$) unless noted differently. Results are displayed as the mean \pm standard deviation (SD). Comparative analysis of group data was performed using two-way ANOVA Test followed by Bonferroni post hoc test for multiple comparisons *via* GraphPad Prism software, with significance determined for P-values under 0.05. *, ** and *** symbols represent the significance level when p value < 0.05, 0.01 and 0.001, respectively.

3. Results

3.1. Hydrogel incubation

Figure 4 illustrates the changes in the dimensions and weight of gelatin hydrogel samples over two weeks of storage in endothelial cell culture medium in an incubator. Samples exhibited significant shrinkage after incubation when compared to non-incubated hydrogels (NI) with a diameter reduction of approximately 18% in average after the first day of incubation, with the dimension remaining relatively stable from day 2 to day 14. Investigating the variations in the weight of hydrogel samples which indicates the shrinkage in the entire volume of hydrogel led to aligned results. The hydrogels showed a substantial initial weight loss of approximately 39% after one day of incubation, followed by stabilization, with minimal further dimensional changes observed over the subsequent days.

3.2. Tensile test

The Young's modulus of the gelatin hydrogel samples during storage in endothelial cell culture medium and incubation in a cell culture incubator is shown in Figure 5. Non-incubated (NI) hydrogels exhibited Young's modulus of 148.2 kPa. After one day of incubation, Young's modulus significantly increased to 327.2 kPa before steadily increasing over the following 14-day incubation period. Between day 1 and day 4, the day-to-day changes in Young's modulus were not statistically significant. However, a significant increase was observed over the incubation period starting from day 1, with Young's modulus rising from 327.2 kPa on day 1 to 529.5 kPa on day 14.

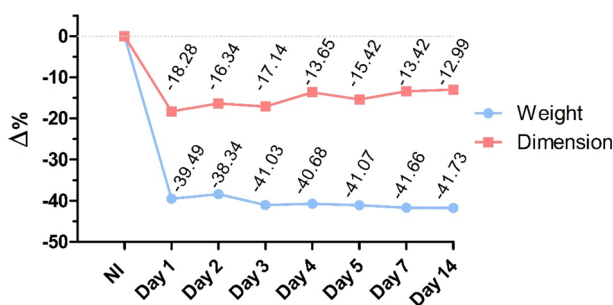


Figure 4. Dimensional and weight changes of gelatin hydrogel samples prior and post-incubation.

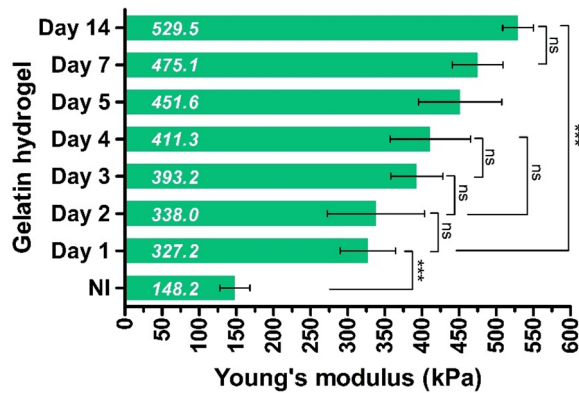


Figure 5. Young's modulus of gelatin hydrogel prior and post-incubation for 14 days.

3.3. Surface characterization: microgroove dimensional analysis

The production precision of microgrooves with widths of 3, 5, 10, 25, 50, and 100 μm and a depth of 1 μm —referred to in this work as geometries 1 to 6, respectively—was evaluated on the PMMA master substrate. The success of their replication onto negative PDMS substrates and hydrogel scaffolds, both before and after incubation in cell culture medium, was assessed by measuring the width and depth of the microgrooves on each substrate. This was aimed to assess the impact of incubation in a cell culture medium on the groove dimensions of surface-engineered scaffolds as well as determine the time point at which scaffold dimensions stabilize, ensuring suitability for cell seeding and minimizing potential effects of shrinking during the cell culture on the cells' behavior.

The results of the characterization of microgroove widths in geometries 1–6 are presented in Figure 6. As shown in the figure, production of the microgroove widths on the PMMA master substrate resulted in slightly larger values than the intended dimensions corresponding to increases of 8%, 3%, 3%, 1.52%, 1.02%, and 0.7% relative to the target values of 3, 5, 10, 25, 50, and 100 μm in geometries 1 to 6, respectively. After successfully replicating the structures from PMMA onto PDMS substrates, the microgroove widths in all geometries slightly decreased, ranging from 9.2% in geometry 1 to 1.5% in geometry 6. This finding suggests that the PDMS solution could fill those small groove spaces on the PMMA substrate during the molding process. Measurements of microgroove widths on non-incubated hydrogel scaffolds (referred as NI in the following figures) showed a slight increase after replication from the PDMS negative mold onto the gelatin hydrogel, presumably due to incomplete filling of the PDMS grooves. Subsequently, the final groove widths on the hydrogel showed no significant difference compared to the PMMA master substrates. This indicates that prior to contact with cell culture medium, the replication process onto the hydrogel scaffolds was carried out with high accuracy. The groove widths on the hydrogel scaffolds decreased significantly after one day of incubation (D1) compared to the non-incubated group (NI). The dimensions on the D1 hydrogel scaffolds with geometries 1–6 reached the mean values of 2.86, 4.69, 9.33, 22.27, 43.42, and 84.20 μm , corresponding to 9.78%, 10.15%, 9.85%, 11.66%, 15.18%, and

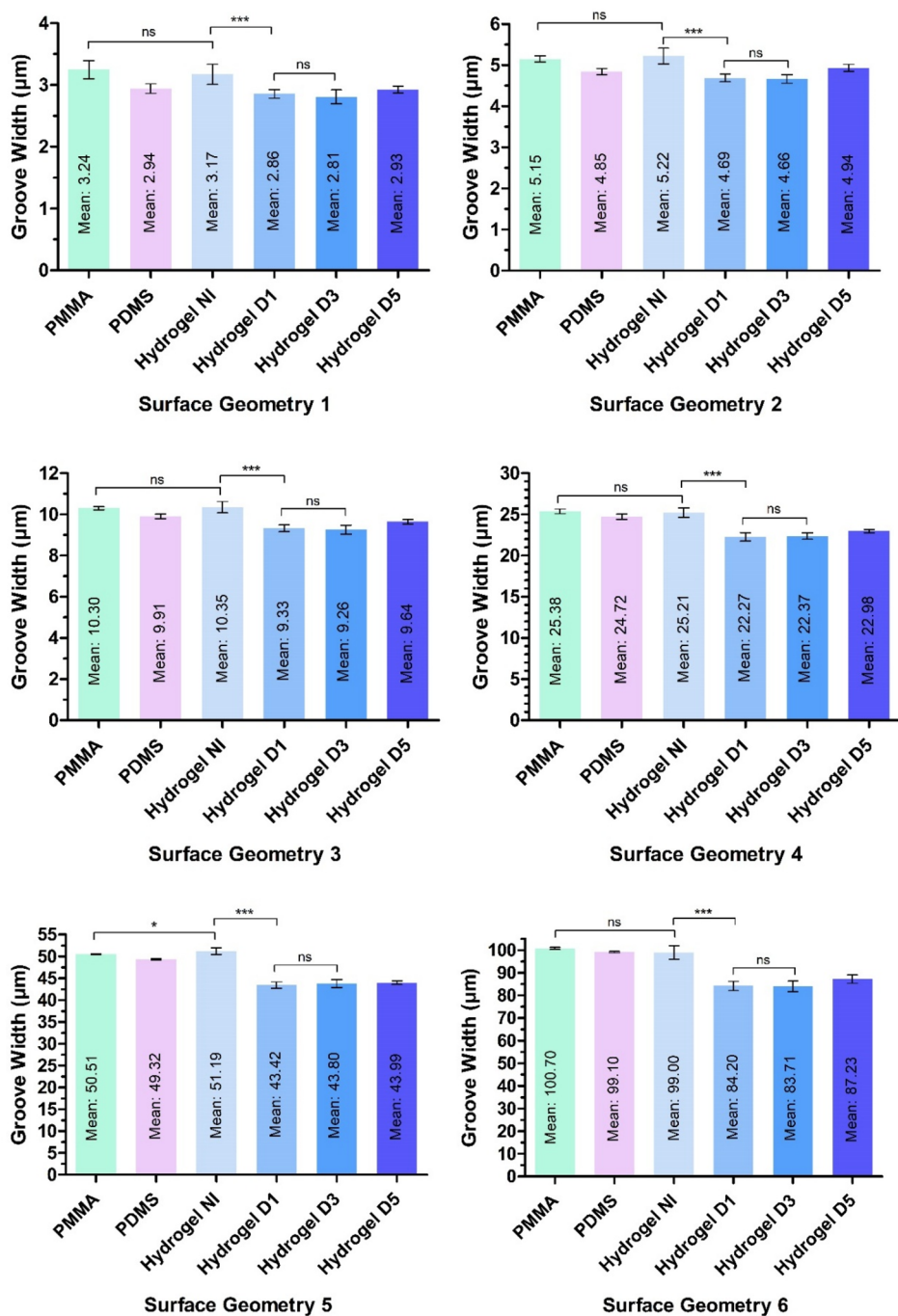


Figure 6. Measured grooves' width on PMMA master substrate, PDMS negative substrate, and gelatin hydrogel prior to and post-incubation for 5 days.

14.94% reduction after incubation, respectively. From that time point onward, the changes in groove width across all the geometries of 1–6 were insignificant and the dimensions stabilized by day 1.

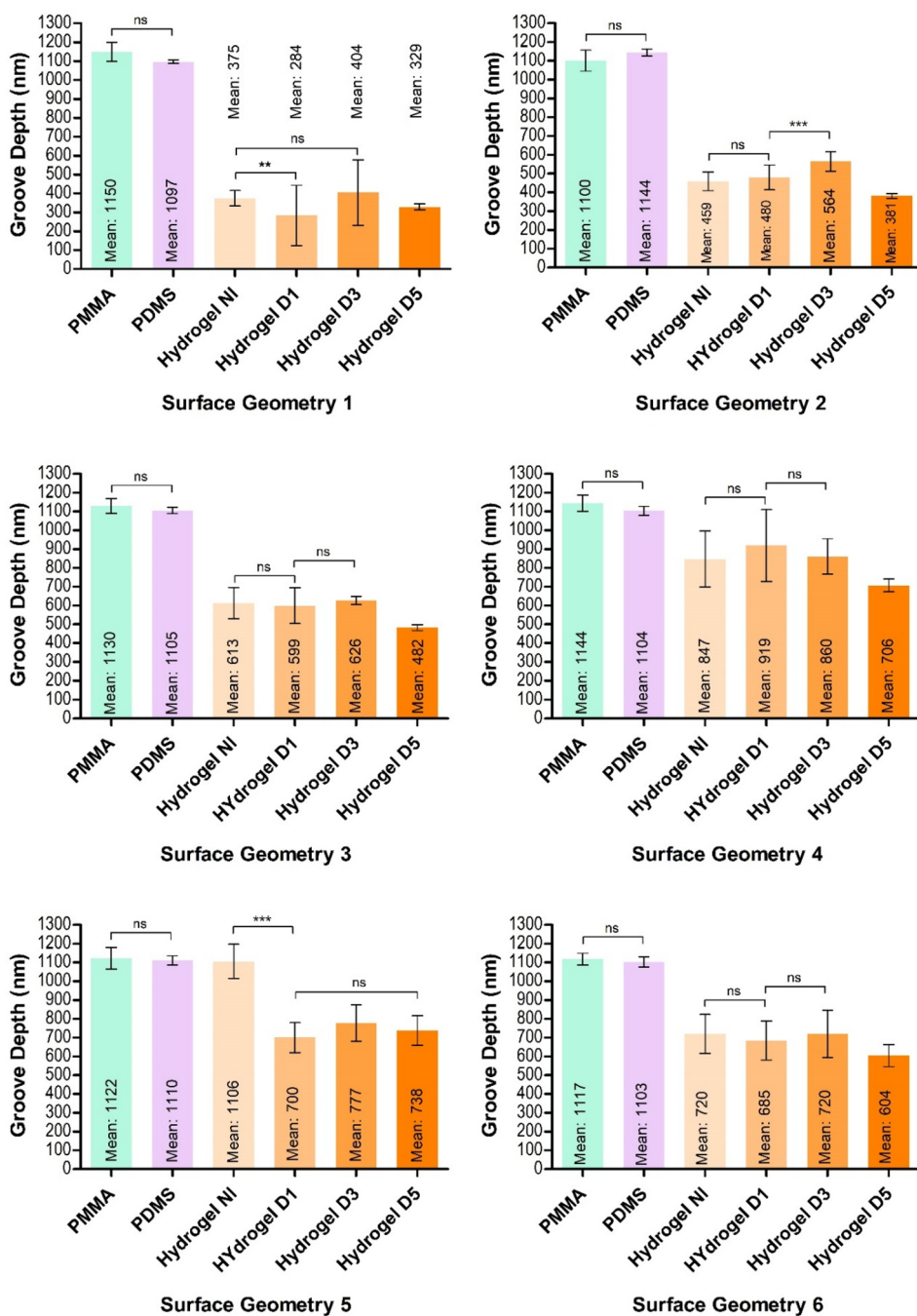


Figure 7. Measured grooves' depth on PMMA master substrate, PDMS negative substrate, and gelatin hydrogel prior to and post-incubation for 5 days.

As illustrated in Figure 7, similar to the phenomenon observed in the replication of widths, the depth production of the microgrooves by laser lithography on the PMMA master substrate resulted in an average 12.7% larger values than the target

dimension of $1\mu\text{m}$. Furthermore, the slight, non-significant difference in the measured depths of the microgrooves between the PMMA and PDMS substrates confirms the effectiveness of the replication method in successfully imprinting depth as small as an average of $1.11 \pm 0.015\mu\text{m}$ onto the PDMS substrate. The depths measurement of the microgrooves on the hydrogel scaffolds prior to incubation (NI) represents reductions of 65.81%, 59.87%, 44.52%, 23.27%, 0.36%, and 34.72%, in geometries 1–6, respectively, compared to the dimensions of the negative PDMS substrate. Comparison of the dimensions of the non-incubated hydrogel (NI) and the hydrogel at day 1 (D1) shows that, alterations in the depth of the microgrooves in geometries 2, 3, 4 and 6 during 1-day incubation in cell culture medium were non-significant. However, the reduction in the depth of grooves in geometries 1 and 5 was notable. Additionally, in geometries 3–6, the minimal depth changes observed after day 1 suggesting that in general, the microgroove depths reached near stability by this time.

3.4. Surface characterization: Microgrooves contour visualization

The 3D graphs of all substrates were obtained using confocal microscopy, and representative images are presented in [supplementary data, Figure S1](#) for geometries 1–3 and [supplementary data, Figure S2](#) for geometries 4–6. The topography of the grooves on all PMMA substrates appears well-defined, with steep sidewalls and clear rectangular profiles that distinctly separate the grooves from the ridges. However, in the smaller grooves of geometries 1 and 2, a slight slope can be observed from the peak of the groove to the bottom. As the groove width increases in geometries 3–6, the sidewalls become noticeably steeper. Interestingly, the microstructures, regardless of their dimensions—from as small as $3\mu\text{m}$ in geometry 1 to as large as $100\mu\text{m}$ in geometry 6—were successfully replicated from the PMMA master substrate onto the PDMS negative substrate without any significant alteration in topography. The replicated structures on PDMS closely resemble the original PMMA profile.

For the hydrogel substrates, in geometries 1–3, starting from the non-incubated hydrogel (H-NI), the sharpness of the structures diminishes after replication from PDMS onto the hydrogel ([Figure 8](#)). The grooves exhibit rounded peaks and valleys, with increased curvature following 1-day incubation. Similarly, the incubated hydrogels on days 3 and 5 show a smooth, wave-like appearance with no sharp edges, indicating substantial softening of the geometry. In geometries 4 and 5, after

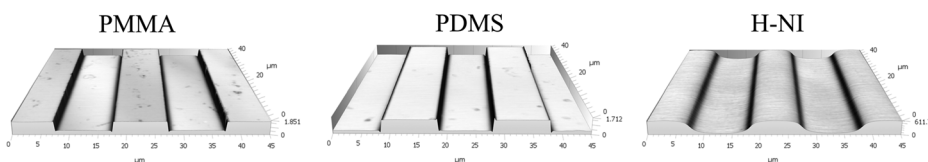


Figure 8. 3D representation of the fabricated SG-3 microgrooves on the PMMA master substrate and replication on PDMS and gelatin hydrogel. Complete surface geometry profiles for all substrates are provided in the [supplementary data](#).

replication onto the gelatin hydrogel, the grooves maintain a more distinct profile, with less noticeable rounding of the peaks and valleys compared to geometries 1–3. The grooves display slight smoothing and rounding over the incubation period; however, the overall profile remains relatively intact, with the grooves maintaining distinct separation and defined depth. In geometry 6, the grooves on hydrogel substrates exhibit negligible rounding or smoothing, even after prolonged incubation (H-D5). The edges remain sharp, and the grooves preserve a clear, rectangular profile, showing the highest stability compared to all other geometries.

Considering all the results collectively, the characterization of the microstructures on the surfaces of hydrogel scaffolds, modified with geometries 1–6, revealed significant changes in the dimensions of the microgrooves during incubation in cell culture medium. Notably, the microgroove dimensions stabilized after 24h of incubation, reaching dimensional stability. These findings underscore the importance of pre-incubating surface-modified hydrogel scaffolds in cell culture medium for 24h prior to seeding endothelial cells. This step is critical to ensure dimensional stability of the scaffolds and to minimize potential effects on cell behavior.

3.5. Surface-modified hydrogel scaffolds

Following the replication of microgrooves from the PMMA master substrate onto the PDMS negative substrate, six distinct geometries were imprinted onto hydrogel scaffolds. These scaffolds were pre-incubated for 24h to stabilize the surface modifications. As a result, six structured hydrogel scaffolds (SG-1–SG-6) with imprinted microgrooves were prepared. In contrast, the control hydrogel scaffold was non-structured (NS), while the tissue culture plate (TCP) with Nunclon Delta surface treatment served as the ideal control condition for cell culture. [Table 1](#) summarizes the characteristics of the surface-modified hydrogel scaffolds prepared for endothelialization.

As shown in [supplementary data, Figure S3](#), a qualitative assessment conducted prior to seeding endothelial cells on the scaffolds, which examined a larger area compared to confocal microscopy, confirmed the presence of microstructures on the surfaces of the surface-modified scaffolds. The microgrooves were successfully imprinted across the entire surface of the gelatin hydrogel scaffolds without defects in replication. Additionally, the boundaries between adjacent grooves were clearly defined and distinctly visible.

3.6. Cell proliferation

[Figure 9](#) illustrates the proliferation of endothelial cells on surface-modified scaffolds with six distinct geometries (SG-1–SG-6), non-structured scaffolds (NS), and the

Table 1. Dimensions of the imprinted microgrooves on the surface-modified hydrogel scaffolds at the time of endothelial cell seeding.

Scaffold	SG-1	SG-2	SG-3	SG-4	SG-5	SG-6	NS
Grooves width (μm)	2.86	4.69	9.33	22.27	43.42	84.20	Non-structured
Grooves depth (nm)	284	480	599	919	700	685	Non-structured

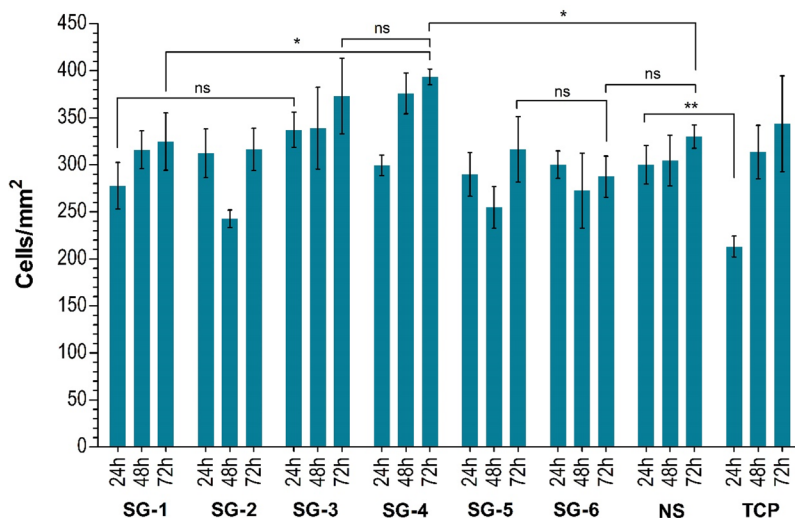


Figure 9. Proliferation of endothelial cells on microstructured, control hydrogel scaffolds (NS) and TCP.

control group (TCP). On the first day of endothelialization, a significantly higher number of cells were observed on all hydrogel scaffolds—both structured and non-structured—compared to the control group. This suggests that gelatin hydrogel scaffolds provide a favorable environment for cell anchorage, outperforming the ideal conditions of the Nunclon Delta surface-treated tissue culture plate (TCP) in the control group. Notably, although SG-3 exhibited a slightly higher cell count at day 1 compared to the other groups, no statistically significant differences were observed between the six structured groups (SG-1–SG-6) and the non-structured scaffold (NS) at this time point.

During the 72-hour endothelialization period, distinct trends were observed among the groups. The number of endothelial cells on SG-1, SG-3, SG-4, and NS consistently increased, aligning with the cell proliferation trend seen in the TCP control group. In contrast, SG-2, SG-5, and SG-6 exhibited a decrease in cell numbers on the second day of endothelialization. Afterward, a slight recovery in cell numbers was observed for these groups by the third day, though the increase was marginal in SG-2 and SG-5 and not statistically significant. In contrast, SG-6 showed only a slight decline in cell numbers on day 3 compared to day 1.

On the final day of endothelialization, SG-4 exhibited the most robust support for cell growth, followed closely by SG-3, with both groups demonstrating the highest proliferation among other surface-engineered and smooth scaffolds as well as the TCP control group. Among the remaining scaffolds, the NS scaffold showed comparable cell numbers to SG-1, SG-2, SG-5, and SG-6, with no statistically significant differences.

3.7. Morphological analysis of endothelial cells

The morphology of endothelial cells cultured on surface-modified hydrogel scaffolds (SG1-6), non-structured scaffolds (NS) and control group (TCP) was assessed by qualitative analysis of fluorescence microscopy images, as Figure 10 represents. On

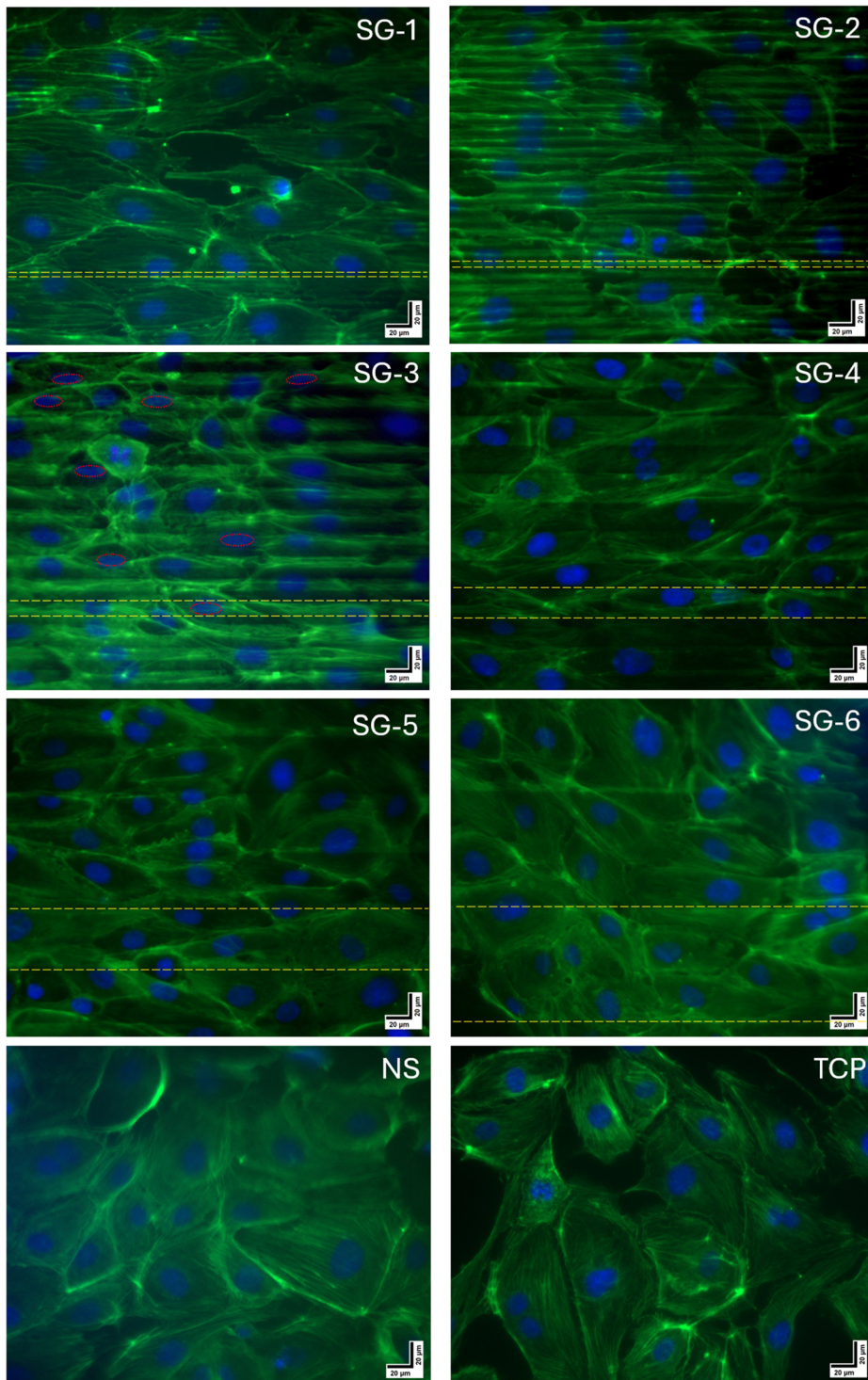


Figure 10. Endothelial cell morphology on the microstructured, control hydrogel scaffolds (NS) and TCP visualized by F-actin and DAPI stainings in green and blue, respectively.

SG-1 and SG-2, actin filaments were more concentrated and pronounced on the bottom of the grooves. Actin filaments on SG-1 and SG-2 seemed to be partly disorganized and fragmented. The cytoskeleton of cells on SG-3 mostly formed compact morphology on the grooves' bottom and cell nuclei displayed noticeable entrapment, with nuclei appearing elongated and confined along the groove channels, as highlighted by red dashed lines in the figure. Actin filaments on SG-3 and SG-4 were shown to be oriented and re-organized in the direction of the grooves while this was not absolutely noticeable in the larger grooves on SG-5 and SG-6. Cells on SG5, SG-6 and non-structured scaffold (NS) showed non-aligned morphology of endothelial cells with actin filaments distributed evenly and nuclei maintaining their typical sub-circular shape comparable to the cells cultured on TCP.

The quantitative evaluation of endothelial cell morphology is presented in Figure 11. As illustrated in Figure 11A, in general, endothelial cells on all microstructured scaffolds (SG-1–SG-6) exhibited significantly lower orientation angles, with mean values ranging from approximately 9.7° on SG-2 to 23.8° on SG-6, compared to the non-structured scaffold (NS) and TCP, which had a mean orientation angle of 69.1° and 68.6° , respectively. The lower angle indicates enhanced alignment of the cells along the direction of the microgrooves on the surface-modified scaffolds, emphasizing the influence of microtopography on cell orientation. Among the microstructured scaffolds,

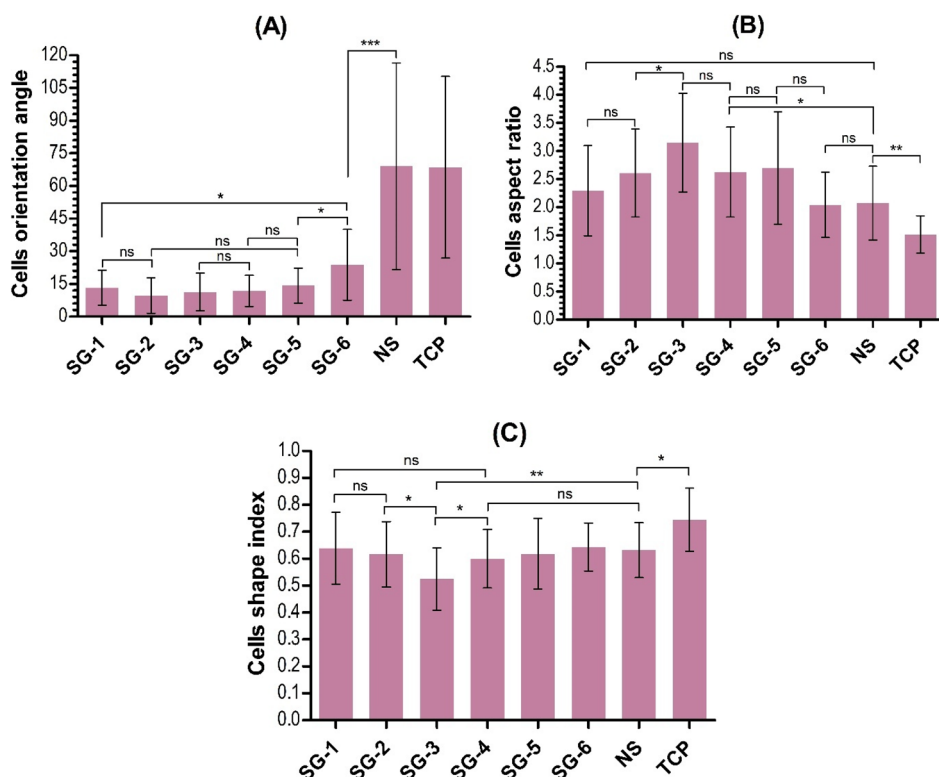


Figure 11. Morphological analysis of the cells on the microstructured (SG), control smooth hydrogel scaffolds (NS) and TCP. (A) Comparison of endothelial cells' orientation angles (A), aspect ratio (B) and Shape indices (C).

cells on SG-2, SG-3, and SG-4 demonstrated the highest alignment along the groove direction. In contrast, a slight reduction in alignment was observed on SG-1 and SG-5, suggesting a reduced effect of the microgrooves on the cells in these scaffolds. While cells on SG-6 exhibited significantly greater alignment than those on smooth scaffolds, their larger orientation angles relative to the groove direction—compared to SG-1 through SG-5—suggest that the microgrooves on this scaffold may be less effective in guiding cell alignment. Considering all the microstructured scaffolds together, cells on SG-6 exhibited a significantly larger orientation angle to SG-1 and SG-5, thus a reduced alignment, while no significant differences were observed among SG-1 to SG-5. Cells on NS and TCP missed a cell orientation, with large standard deviations in orientation angles highlighting the completely random cell orientation in the absence of topographical cues.

The aspect ratio of endothelial cells, indicative of cell elongation, on the different substrates is presented in [Figure 11B](#). The highest elongation was observed on SG-3, with an aspect ratio of 3.1, followed by SG-2, SG-4, and SG-5, each with an aspect ratio of approximately 2.6. These values were significantly higher than those of cells on the NS scaffolds and in the TCP control groups, demonstrating the impact of the microgrooves on cell elongation. Conversely, the negligible difference in the measured mean aspect ratios between SG-1 (2.2) and SG-6 (2.04) compared to the NS control scaffold (2.07) suggests that the microgrooves in these scaffolds did not significantly influence cell elongation. The shape index analysis, which is indicative of cellular circularity, reflects not only elongation but also potential irregularities in cell boundaries during various spreading patterns across the scaffolds. As shown in [Figure 11C](#), except for SG-3, cells on all structured scaffolds exhibited similar shape indexes, ranging from 0.60 to 0.64, with no significant differences either among them or compared to the non-structured scaffold (shape index 0.63). The cells on SG-3, however, had the lowest shape index among all groups with a shape index of 0.52 which may be indicative of a more elongated or irregular morphology. On TCP, the cells exhibited the highest circularity among all the substrates with the shape index of 0.75.

3.8. Vinculin and VE-cadherin expression

The average fluorescence intensity of vinculin protein, localized in the focal adhesion complexes associated with cell-to-matrix junctions, was measured in endothelial cells cultured on non-structured hydrogel scaffolds (NS) as the control group and structured scaffolds with six distinct geometries at the final day of endothelialization. The relative expression of vinculin, normalized to the fluorescence intensity of the NS group, is shown in [Figure 12A](#). Endothelial cells on SG-1 and SG-2 exhibited similar vinculin expression levels, with approximately 1.19 and 1.12-fold normalized expression, respectively, which were higher than the smooth hydrogel scaffold as control. SG-4 demonstrated the highest vinculin expression, with nearly a 2-fold increase compared to the NS scaffold followed by 1.61- and 1.58-fold vinculin expression on SG-3 and SG-5, respectively. Notably, SG-6 did not show a significant increase in vinculin expression relative to the NS group.

[Figure 12B](#) presents the relative VE-cadherin expression levels, normalized to the fluorescence intensity of the NS control group. In general, endothelial cells on SG-1

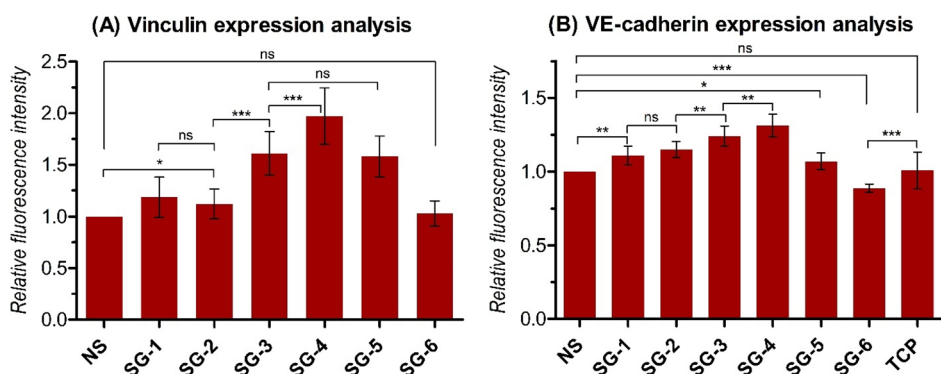


Figure 12. Expression of Vinculin and VE-cadherin from endothelial cells on control (NS) and surface-structured hydrogel scaffolds.

to SG-5 expressed higher VE-cadherin compared to the control smooth (NS) hydrogel scaffold. SG-1 and SG-2 showed an increase (1.11-fold and 1.15-fold, respectively), with no statistically significant difference between them. SG-3 and SG-4 showed a significant increase, with SG-4 exhibiting the highest expression level at 1.31-fold relative to the NS group. In contrast, the expression in SG-6 was the lowest, 0.88-fold compared to control smooth hydrogel. Figure 13 displays VE-cadherin expression (stained in red), highlighting the cohesion and cell-to-cell junctions of endothelial cells on the final day of endothelialization. In general, VE-cadherin-positive HUVECs were observed across all structured scaffolds (SG-1 to SG-6), the non-structured (NS) scaffold, and the TCP control group. The boundaries of cells appear aligned with the groove direction on substrates SG-1 to SG-5, proving cellular alignment along these features, whereas this was not observed on the other substrates. Uniform development of cell-cell junctions in VE-cadherin positive cells was evident on scaffolds SG-1 to SG-5 and the NS scaffold, comparable to the TCP control, indicating the formation of a confluent endothelial monolayer covering the entire surface of these substrates. In contrast, on SG-6, partial development of endothelial cell monolayer was evident with visible small cell-free gaps.

4. Discussion

In this study, we present an uncomplicated replication method, in contrast to more complex techniques in previous works, for generating a diverse range of microgroove dimensions on hydrogel scaffolds, addressing the limitations of previous approaches and expanding the understanding of surface engineering for improved endothelialization. Reported technologies for the fabrication of structured hydrogels, including 3D bioprinting [42], electrospinning [43], and microfluidic spinning [46] require complex manufacturing processes and involve high equipment costs. The application of 3D bioprinting is limited by material selection, poor mechanical properties, and low resolution. Electrospinning lacks precise control over fiber dimensions and often involves toxic solvents. Moreover, the extensive pre- and post-processing requirements, along with the limited scalability and reproducibility of microfluidic technology for structuring hydrogels, restrict its broader application. This work characterizes the mechanical

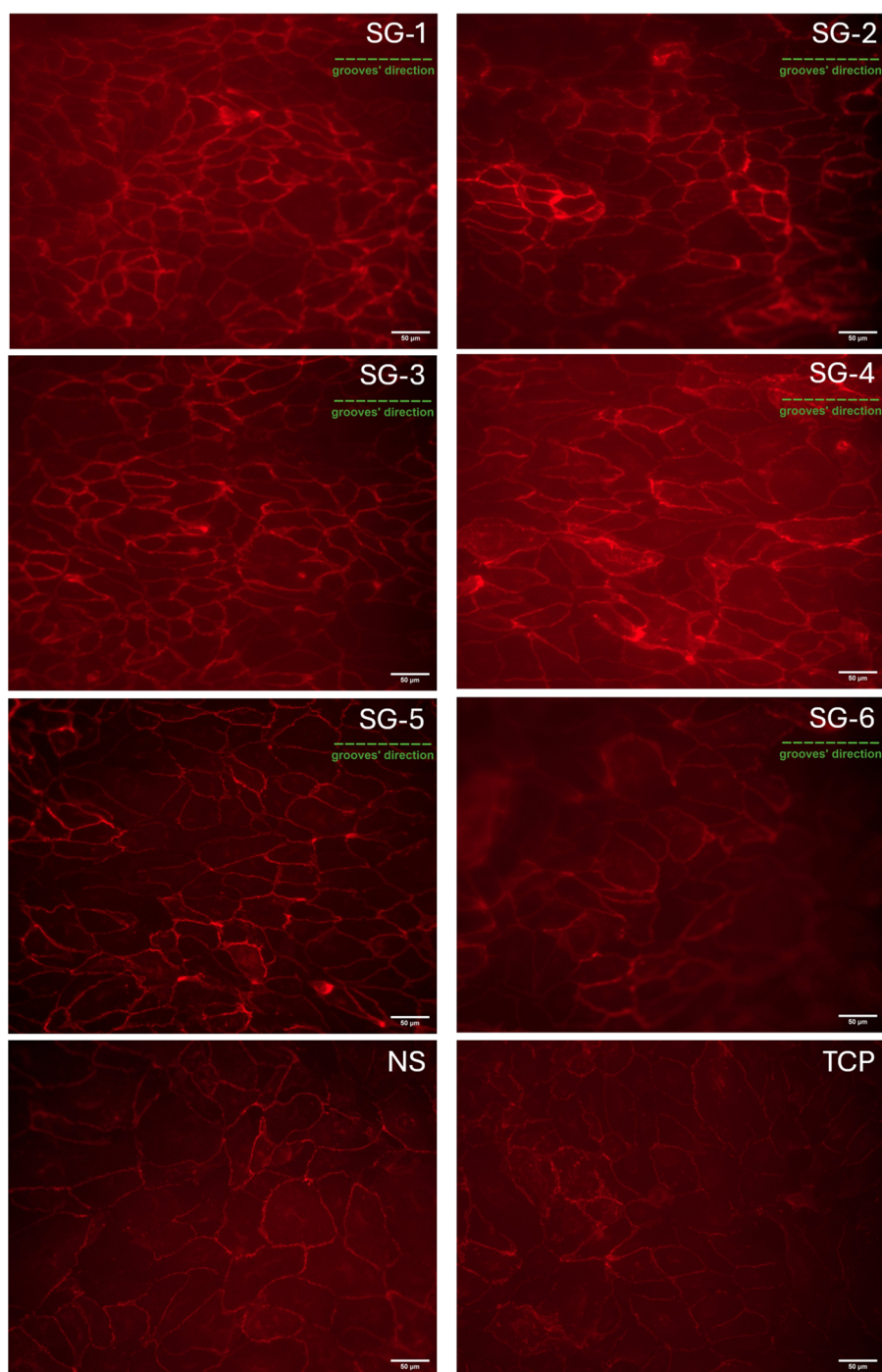


Figure 13. Endothelial cells' VE-Cadherin expression on control (NS), surface-structured hydrogel scaffolds and TCP visualized in red signals.

properties and engineered surface topography of mTG-crosslinked gelatin hydrogels, which incorporate a biocompatible crosslinker with no risk of toxic residues during the crosslinking process, before and after incubation in a physiologically simulated

environment with cell culture medium at 37°C. Furthermore, we explore the alterations in the hydrogel's properties over an extended period and provide a comprehensive assessment of their impact on endothelial cell proliferation, morphology, cell-substrate interactions, and endothelium formation aiming to advance the understanding of surface engineering strategies for hydrogel scaffolds in vascular tissue engineering applications. Tissue engineering focuses on tailoring surface-modified biomaterials to fabricate biomimetic scaffolds and optimized intravascular implants, supporting *in vitro* research and applications in regenerative medicine [47–50]. A thorough understanding of the complex interactions between cells and biomaterial surfaces is crucial for effective surface engineering. Improving the design of vascular grafts and endovascular devices can be achieved by studying the interactions between endothelial cells and scaffolds with engineered microtopographies, along with the ability to control endothelial cell morphology and orientation. Endothelialization of intravascular scaffolds enhances the hemocompatibility and anti-thrombotic performance of these biomaterials [51]. Surface engineering facilitates rapid endothelialization of biomaterials upon *in vivo* implantation which is crucial for the long-term patency of vascular grafts, as it helps prevent acute thrombosis and inhibits smooth muscle cell hyperplasia [52,53]. Yi et al. demonstrated that introducing 20µm wide microgrooves onto the surface of electrospun grafts accelerates the formation of a native-like endothelium but also effectively reduces platelet aggregation and inflammatory responses when compared to grafts without surface modifications, as observed *in vivo* [54]. Sprague et al. demonstrated that coronary stents with microgrooves (~15µm wide, 2µm deep) enhanced endothelial function in a porcine model by promoting cell proliferation, nitric oxide production, and reducing apoptosis. This surface modification supported endothelial migration, preserved anti-inflammatory function, and reduced neointimal formation, with no expression of proinflammatory markers like VCAM or TNF-alpha [51].

In vascular tissue engineering, a primary objective is to draw inspiration from the physical properties of the vascular ECM in order to replicate its three-dimensional architecture, which provides structural support for cells. Nanoscale geometries of ECM influence the organization of cell adhesion molecule receptors at the sub-cellular level, while microscale geometries impact supra-cellular properties such as cell morphology, proliferation, and migration [20]. Notably, microstructural analyses reveal that the surface topography of natural blood vessels exhibits microgroove-like features, with endothelial cells aligning along these grooves in the direction of vessel's longitudinal axis [55]. The subendothelial basement membrane of blood vessels contains nanoscale fibers with a thickness of approximately 50–100 nm [56]. This fibrous membrane is further organized into larger, longitudinally oriented microscale ridges and grooves on the luminal vessel surface, with estimated widths of several hundred micrometers [57]. Therefore, this study selected a groove-and-ridge topography incorporating both nano- and micro-scale features—specifically, micro-scale groove widths combined with nano-scale depths—as the surface modification strategy for gelatin hydrogel scaffolds, aiming to mimic the natural microenvironment of endothelial cells in blood vessels. Furthermore, the interaction of HUVEC with the modified scaffolds was investigated following analysis of the physical and mechanical properties of the material over an extended period under simulated cell culture conditions in order to gain deeper insights into its interaction with the surrounding environment.

Understanding the mechanical and physical alterations of gelatin hydrogels in cell culture conditions is essential for optimizing their application in tissue engineering. While previous studies have primarily investigated the impact of hydrogel incubation on swelling/shrinkage behavior in solutions such as PBS and water under different temperatures [58–60], our study explores the effects in real cell culture conditions. Specifically, we examined the influence of endothelial cell culture medium on hydrogel scaffolds, following sterilization, under physiological conditions in cell culture medium and in a cell culture incubator for 14 days. When gelatin hydrogels are immersed in aqueous environments, swelling occurs due to the interactions of NH_2 , COOH groups and free $-\text{OH}$ groups in gelatin hydrogel structure, forming hydrogen bonds with water molecules [61]. The degree of swelling is strongly influenced by factors such as ionic composition and pH of the surrounding solution, gelatin concentration, and crosslinking method [62]. The 39.49% decrease in weight and 18.28% decrease in dimensions observed during the first day of incubation of the samples reflect an initial rapid loss of water from the hydrogel that should be due to changes in polymer-solvent interactions as hydrogels adjust to the ionic composition and pH of cell culture medium. This shrinkage of gelatin hydrogel under the physiological environment in our study was aligned with the findings of previous studies [63,64]. The observed shrinkage in the hydrogel samples could be due to osmosis. The ionic strength of the cell culture medium, defined by the total concentration of dissolved ions, increases the osmotic pressure around the hydrogel, reducing its ability to retain water. Another widely discussed phenomenon in previous studies is that cell culture medium contains salts, such as sodium chloride, potassium chloride, calcium chloride, and bicarbonates, which together establish a specific ionic strength. Ions in the culture medium, such as Na^+ and Cl^- , tend to form hydration shells and compete with the hydrophilic sites on the gelatin hydrogel, attracting water molecules. This competition disrupts and weakens the hydrogen bonds between water and the hydrophilic groups of the gelatin matrix, leading to shrinkage [65,66]. Moreover, the shrinkage of the gelatin hydrogel in our study could be due to the ionic shielding by the cell culture medium's salts. At the physiological pH of 7.4 of the cell culture medium, carboxyl groups (COO^-) and amino groups (NH_3^+) in the gelatin network experience reduced electrostatic repulsion. This occurs because the charged functional groups of gelatin are surrounded by dissolved ions from the medium, which neutralize their charges and subsequently diminish the electrostatic repulsion between them. Weakening repulsive forces between similarly charged groups in hydrogel allows the polymer chains to come closer together and further compact the networks causing overall shrinkage [67–69]. After the first day of incubation, the hydrogel reaches an equilibrium state, as evidenced by the stabilization of weight loss and dimensional reduction that can reflect a balance between osmotic and elastic forces, wherein the polymer network resists further compaction.

The Young's modulus (E) of gelatin hydrogels can be modulated over a wide range, from very soft ($E=1.5\text{ kPa}$) to highly rigid ($E>600\text{ kPa}$), allowing for precise control of their stiffness [70]. The steady increase in Young's modulus from 148.2 kPa (non-incubated hydrogels) to 529.5 kPa (Day 14) underscores the progressive stiffening of the hydrogels during incubation. The observed trend of increasing Young's modulus and decrease in swelling can primarily be attributed to the intrinsic

relationship between the swelling behavior and mechanical performance of hydrogels [71]. Furthermore, as discussed earlier, the influences of ionic composition and pH of the medium possibly reduced electrostatic repulsion between COO^- and NH_3^+ groups, compacting the network and contributing to higher Young's modulus values [61,64]. Residual mTG activity during incubation at 37°C could further strengthen the hydrogel network over time. Additionally, the ionic environment of the medium may have facilitated secondary interactions, such as ionic crosslinking or salt bridging, between charged groups in the gelatin matrix, further enhancing the mechanical properties over 14 days. Although the Young's modulus of the gelatin hydrogel increased steadily during contact with the culture medium, from 327.2 kPa on the first day of incubation to 529.5 kPa on day 14, this remains within the range of natural blood vessel mechanics, which vary from 200 kPa to 1 MPa depending on the origin of the vessel [72–76].

Laser lithography was chosen as the preferred technology for fabricating surface topographies on PMMA substrates, featuring parallel grooves and ridges with symmetric spacing and fine dimensions ranging from widths of $3\text{ }\mu\text{m}$ to $100\text{ }\mu\text{m}$ and depth of $1\text{ }\mu\text{m}$. This method demonstrated high reliability for the production of micropatterns on the master PMMA substrate. Production accuracy of groove widths on PMMA sheets increased with groove size, improving from 92% for $3\text{ }\mu\text{m}$ grooves to 99.3% for $100\text{ }\mu\text{m}$ grooves. Similarly, depth production accuracy increased from 85% for $3\text{ }\mu\text{m}$ grooves to 98.3% for $100\text{ }\mu\text{m}$ grooves. In addition to preserving the quality of the PMMA substrates for repeated replication, the use of flexible PDMS as an intermediate mold also enables future applications, such as structuring the inner surface of tubular hydrogels by wrapping it around cores and placing them in cylindrical molds. The microstructures were successfully replicated onto PDMS negative substrates without any noticeable variation in dimensions. The imprinting accuracy of groove widths on gelatin hydrogel scaffolds generally improved with increasing geometric dimensions, achieving the accuracy of 92.18%, 92.38%, 93.57%, 98.02%, and 99.99% for geometries 1 to 6, respectively. Similarly, the imprinting accuracy for groove depths increased with groove width, from 34.18% for geometry 1 and reaching a maximum of 98.75% for geometry 5. The low depth replication accuracy in the narrower grooves may be due to the fact that the transfer of micropatterns from molds to gelatin hydrogels is often hindered by the high viscosity of the gelatin solution. This high viscosity limits the flow of the solution into the negative template structures and complicates template separation, particularly at such a high gelatin concentration in the hydrogel solution [64]. During the incubation of microstructured hydrogel scaffolds in cell culture medium, significant shrinkage of the microgrooves was observed by day 1, consistent with our findings from hydrogel incubation tests on cylindrical samples. After day 1, the groove dimensions stabilized, suggesting that the imprinted topographies on the scaffolds reached equilibrium within the first day of incubation. Therefore, endothelialization experiments were conducted after a 24-hour pre-incubation of the scaffolds in cell culture medium within the incubator. This pre-incubation step was intended to minimize the potential stress induced by surface topography changes, thereby reducing its impact on the seeded cells on the surface-modified scaffolds. Despite shrinkage, the final dimensions of the grooves on the scaffolds successfully met our objective of creating submicron-deep grooves

ranging in widths from 2.86 μm to 84.2 μm . Selecting a range of groove dimensions encompassing those reported in previous studies provides a more comprehensive analysis of topographical effects on endothelial cell behavior. This range encompasses the reported effective groove dimensions for promoting endothelialization, which spans from 2 μm to 100 μm in width and submicron depth [77–81]. These scaffolds were designed to compare the influence of groove dimensions on the endothelialization of gelatin hydrogels crosslinked with mTG, thereby identifying the optimal groove size for this specific application.

Surface topography plays a significant role in modulating cell function, as evidenced by changes in cell morphology and alignment on substrates with microscale and nanoscale patterns [18,82]. The changes in the organization of actin filaments that lead to morphological alterations can regulate the cell functions including proliferation, apoptosis, differentiation, nitric oxide production, and expression of the inflammatory-related gene of ICAM in endothelial cells [83–87]. It is important to provide a microenvironment for endothelial cells that supports their natural morphology, even in the absence of fluid shear stress, as the regulation of cell shape and cytoskeletal organization is essential for normal cell function and immunogenic responses [27]. Morphological analysis of HUVECs after 24 h revealed that microgrooves of different geometries have distinct influences on the cells. On grooves with widths less than 5 μm and with depths less than 500 nm (SG-1-2), actin filaments of individual cells were more pronounced at the bottom of the grooves, and the cells were able to span across to adjacent grooves. In SG-3, with a width of 9.33 μm and a depth of 599 nm, the cell nuclei were reshaped by the physical constraints of the groove walls, resulting in nuclear entrapment within the grooves. Such nuclear deformation due to topographical influence might impact endothelial cells by altering chromatin organization and therefore changing cell behavior, gene expression patterns, and triggering downstream signaling processes [88–90]. The elevated presence of actin filaments on the bottom of the groove is potentially due to mechanical constraints caused by insufficient space for proper cellular spreading imposed by the microstructure. In contrast, cells on larger grooves on SG-4 to SG-5 shaped a spindle-like morphology and exhibited more organized actin filaments elongated in the direction of grooves, with no signs of impaired morphology, and cells were able to bridge between grooves and ridges effectively. Endothelial cells on SG-6 (groove width of 84.20, depth of 685 nm) and the flat substrates of NS and TCP showed a morphology similar to the typical endothelial cells that exhibit a cobblestone appearance with randomly oriented actin fibers [91].

Anisotropic topographical cues promote the elongation of cellular focal adhesions along the axis of the topographic pattern while limiting their growth in the perpendicular direction. This spatial organization drives the alignment of actin stress fibers, orienting and elongating cells along the topography [44]. Dunn et al. explained that actin filaments tend to form in straight lines, preventing fibers from spanning across the groove sidewalls and resulting in alignment parallel to the grooves, which elongates the cells [92]. Quantitative analysis of endothelial cell morphology on the scaffolds demonstrated that surface modifications with microgrooves in SG-1 to SG-6 significantly enhanced HUVEC alignment, with orientation angles ranging from 9.7° to 23.8°. This effect was less pronounced in the larger grooves of SG-6, which had a

width of 84.20 μm , likely because the topographical features exceeded the dimensions of individual cells. Endothelial cells in blood vessels are approximately 15 μm wide and 50 μm long, with HUVEC thickness reported as 5 μm at the nucleus and 3 μm in the non-nuclear region [77,93]. The observed cell alignment in this study is consistent with previous findings, where endothelial cells exhibited orientation angles of 18° and 6.9° on grooves 5 μm wide and 1 μm deep, and 13° on grooves 10 μm wide and 1 μm deep [94,95]. Endothelial cell elongation on SG-2 to SG-5 scaffolds was greater than on the control smooth hydrogel scaffold, with aspect ratios averaging approximately 2.6 compared to 2.07 in the non-structured (NS) control. The highest elongation was observed on the SG-3 scaffold, with an aspect ratio of 3.1. In contrast, microgrooves with very small dimensions (2.86 μm width and 284 nm depth in SG-1) and very large dimensions (84.2 μm width and 685 nm depth in SG-6) did not effectively facilitate endothelial cell elongation. This observation aligns with findings by Sun et al. who reported that endothelial cells exhibited an aspect ratio of 2.5 on microgroove scaffolds with a 50 μm radius of curvature, decreasing to an aspect ratio of 2 as the groove width increased to 75 μm [96]. The shape index of endothelial cells *in vivo* is reported to be around 0.34–0.53 depending on the position of cells *in vivo* [97]. A similar shape index was observed on surface-modified scaffolds (0.52–0.64) compared to the smooth control scaffold (0.63) and TCP (0.75). This similarity suggests that the imprinted microgrooves on the scaffolds did not induce cell shape irregularities or disrupt normal cell spreading. Consistent with this, previous studies reported endothelial cell shape indices ranging from 0.5 to 0.61 on grooves with widths of 3, 5, 10, and 30 μm [27,79].

The geometry and width of microgrooves play a critical role in regulating endothelial cell proliferation. Quantification of endothelial cell proliferation on surface-modified scaffolds with geometries 1–6 and control groups indicated that microgrooves in geometries 3 and 4 significantly enhanced HUVEC proliferation. Geometry 3 featured a width of 9.33 μm and a depth of 599 nm, while geometry 4 had a width of 22.27 μm and a depth of 919 nm. These specific dimensions outperformed other groove configurations, flat hydrogel scaffolds, and the TCP control group in promoting cell proliferation. Similarly, Lu et al. studied the growth of rat aortic endothelial cells on patterned titanium surfaces featuring microgrooves with widths ranging from 750 nm to 100 μm and depths of less than 200 nm. Their findings revealed that cell proliferation and viability were enhanced on 20 μm grooves and the lowest proliferation was observed on 100 μm grooves [98]. Moreover, a comparative endothelialization study on different grooves widths of 3, 5, 10, 30 micrometers showed that after 2 days, the highest number of cells among the microgrooved surfaces was detected on 30-micrometers grooves [79]. Previously, promotion in endothelial cell proliferation on Ti surfaces with 25-micrometers grooves has been shown [99,100]. While we did not observe enhanced endothelialization on wider grooves (SG-5 and SG-6 = 43.42 and 84.2 μm , respectively) Govindarajan et al. demonstrated that endothelial cells attach and proliferate up to 30% more on microgrooved shape-memory polymer scaffolds with a 50-micrometers width and a depth of approximately 400–500 nm [101].

The anchorage of endothelial cells to substrates is facilitated by the interaction of integrins with focal adhesion complexes (FACs), which include proteins such as

Vinculin [102]. Assessment of Vinculin expression from cells could provide insight into cell-substrate adhesion strength [103]. In our study, microgrooved hydrogel scaffolds generally enhanced Vinculin expression compared to smooth scaffolds. Vinculin expression increased progressively as the microgroove dimensions expanded from 2.86 μm in width and 284 nm in depth (SG-1), reaching a peak in SG-4 with grooves measuring 22.27 μm in width and 919 nm in depth. However, larger grooves exhibited less effectiveness in enhancing Vinculin expression, as SG-6 showed no improvement in Vinculin expression compared to the flat control substrate. Similarly, Kooten et al. demonstrated that HUVECs cultured on silicon substrates with channel depths of 500 nm and widths of 2, 5, and 10 micrometers exhibited significantly increased expression of Vinculin [104]. Moreover, higher expression of Vinculin by microgrooves with widths of 5, 10 and 20 micrometers and submicron depth has been reported in fibroblasts [92,105]. VE-cadherin, a key transmembrane protein exclusively expressed in endothelial cells, essential for supporting tight junction formation, was present in cells on all surface-modified scaffolds and the control group [106]. Imaging of VE-cadherin to evaluate the integrity of the endothelial cell monolayer revealed fine cell-to-cell adhesion in microgrooved scaffolds, comparable to that observed in smooth scaffolds and TCP control group. A more compact endothelium was visible on smaller grooves on SG-1 to SG-5 while HUVECs exhibited more spreading on SG-6, non-structured scaffolds and TCP. The lack of neighboring cell junctions could be seen in a few areas of SG-6 suggesting delayed endothelial maturation compared to other substrates. This observation is supported by the VE-cadherin expression data, with SG-3 and SG-4 showing the highest expression levels, indicating enhanced formation of intercellular junctions. In contrast, SG-6 exhibited the lowest VE-cadherin expression, reflecting impaired junctional integrity. The comparable VE-cadherin levels between cells on smooth hydrogel scaffolds and those on TCP indicate that the hydrogel substrate itself does not negatively affect VE-cadherin expression in endothelial cells. The decrease in the number of cells from day 1 to day 3 and immature coverage of endothelial cells in SG-6 may be attributed to findings by Fernández-Castillejo et al. who reported that grooves with sharp sidewalls hinder the growth of endothelial cells compared to slope-shaped grooves [107]. The sharp edges of the grooves on SG-6 may have inhibited cell proliferation, while the grooves on the other scaffolds featured sloped sidewalls that seamlessly connected the groove bottoms to the ridges, potentially facilitating better cell growth and migration.

Surface engineering with microgrooves provides even more benefits than increasing cell proliferation, endothelium maturation, and guiding cell elongation and alignment. Microgrooves can also influence the viability of endothelial cells. Wu et al. reported that 15 μm grooves induced apoptosis in cells, whereas cells remained viable on wider 25 μm grooves [108]. Chen et al. showed that endothelial cells on 30 μm microgrooves compared to 3, 5 and 10 μm expressed the highest levels of eNOS and CD3, supporting enhanced cell function and a healthy phenotype. Additionally, these grooves extended prothrombin time (PT) and activated partial thromboplastin time (aPTT), indicating reduced thrombogenic potential [79]. The cobblestone-like morphology of endothelial cells with randomly oriented actin filaments in SG-6, NS and TCP substrates is to some extent similar to the athero-prone phenotype of endothelial cells commonly observed in hemostasis *in vivo* [30,32]. However, the elongated and

aligned cell morphology with organized actin filaments observed on SG-1 to SG-5 aligns with previous findings emphasizing the importance of such morphology for maintaining healthy endothelial cell function with suppressed monocyte activation [109]. Endothelial cells exhibiting similar elongated morphology, resembling their natural state in blood vessels, demonstrated a significant five-fold reduction in monocyte recruitment and an eight-fold decrease in the release of monocyte chemotactic protein-1 (MCP-1) when cultured on 3D scaffolds compared to flat 2D substrates [110].

Given that cellular responses are highly dependent on feature geometry, material properties, and cell type, findings from prior studies—often conducted on varying cell types, materials, and surface topographies—cannot be universally extrapolated to our specific cell type and material. While studies on the surface modification of gelatin hydrogels with microgrooves to investigate cell-substrate interactions are limited, to the best of our knowledge, no research has explored the micropatterning of mTG-crosslinked gelatin hydrogels across a wide range of groove dimensions and their influence on HUVECs. Jeon et al. fabricated grooves with a single width of $45.5\mu\text{m}$ and a ridge depth of $50.7\mu\text{m}$ on mTG-crosslinked gelatin hydrogels stabilized on a PDMS substrate to study myoblast differentiation into myotubes [111]. However, their characterization of groove dimensions by SEM imaging under dry conditions on the first day only provides limited insight into dimensional changes over time during cell culture. Furthermore, systematic studies on the mechanical property alterations of gelatin hydrogels before, during, and after incubation in cell culture medium remain absent. Tadsen et al. investigated the fabrication of microgrooved surface topographies with a single width of $3.75\mu\text{m}$ and a depth of 800nm on gelatin hydrogels crosslinked by electron beam [64]. Their study examined the effects of gelatin concentration and irradiation dose on pattern fidelity, as well as the influence of surface structuring on 10% wt hydrogels on fibroblast and endothelial cell behavior. Electron beam crosslinking caused notable shrinkage, with reductions of 14% and 8% in 4wt% and 10wt% gelatin hydrogels, respectively. The structure heights were consistently lower than the intended 800nm in the template, ranging from 200 to 400nm in 4–6wt% hydrogels and exceeding 500nm in 12–14wt% hydrogels. Significant shrinkage of the structures was observed during the first day in PBS storage, followed by stabilization, which aligns with our findings on surface characterization during a 5-day incubation in the culture medium. However, structural characterization was conducted in PBS, thus not under cell culture conditions in an endothelial cell culture medium, and was limited to a small number of replicates ($n=2$), which even displayed slightly different trends in swelling during early incubation. Additionally, the mechanical properties of the hydrogels were not analyzed. The significantly lower cell density on modified hydrogel scaffolds compared to controls, coupled with the lack of additional cellular experiments (e.g. VE-cadherin expression, cell-substrate attachment strength, and quantification of cell morphological changes), limits understanding of the effectiveness of these surface modifications on gelatin hydrogel scaffolds.

While our study aimed to characterize different surface topographies on gelatin hydrogel scaffolds and investigate their endothelialization, several limitations should be considered. The Young's moduli of gelatin hydrogel in our study increased constantly during the incubation period. Given that scaffold stiffness affects cell behavior

[112], chemically preventing hydrogel network compaction due to ionic interaction, as well as inhibiting the continued activity of residual mTG during incubation, may result in more stable mechanical properties. Consequently, such approaches would eliminate the cross-effect of increasing surface stiffness on endothelialization, even though this increase in Young's modulus was consistent in all the hydrogel scaffolds and therefore does not undermine the validity of our comparative assessment of endothelialization on the various surface-modified scaffolds. While achieving nanoscale depth for microgrooves on gelatin hydrogel scaffolds successfully fulfilled the primary objective of this study, the replication accuracy was uneven due to the high viscosity of the gelatin solution, which impeded its flow into smaller grooves. Future optimization of the replication process could address this limitation, ensuring consistent groove depth and eliminating variations associated with different groove width dimensions and possible influence on endothelialization. Additionally, adjusting groove depth in other dimensions could enable future studies to isolate and investigate its specific impact on the production process and endothelialization.

Future studies could focus on investigating the endothelialization of the surface-modified scaffolds over extended time periods and employing more robust assays, such as XTT, to evaluate cell proliferation more comprehensively. Since endothelial cell morphology and alignment are closely linked to their functionality, future studies could investigate the secretion of immunomodulatory factors by endothelial cells cultured on microgrooved scaffolds. Comparisons with smooth scaffolds and TCP would provide valuable insights into the impact of scaffold topography on cellular behavior. Upon reviewing the outcome of our study, we see possibilities for further investigations into endothelial cell behavior on the introduced surface-modified scaffolds under physiological flow conditions and thus shear stress aiming to evaluate the impact of the developed surface topographies on enhancing endothelialization. Looking ahead, we acknowledge possibilities for implementation of the surface topographies on the outer as well as on the luminal surface of tubular scaffolds, vascular grafts and stents to improve the endothelialization process.

5. Conclusion

Our work introduces a reproducible method for producing microgroove topographies on gelatin hydrogel scaffolds by replicating structures from a PMMA substrate onto a PDMS substrate, followed by imprinting onto the hydrogel. The scaffolds were further subjected to physical and mechanical characterization in a physiologically simulated environment. To the best of our knowledge, this study is the first to investigate the interaction of HUVECs with enzymatically crosslinked 13% gelatin hydrogel scaffolds, evaluating cell proliferation, morphological characteristics, and the expression of vinculin and VE-cadherin across a wide range of microgroove dimensions.

The prepared gelatin hydrogels exhibited Young's modulus of approximately 327–530 kPa over 14 days of incubation, aligning with natural vessel mechanics. The microgrooves achieved over 92% width accuracy and up to 98% depth accuracy in larger topographies. The stabilization of hydrogel dimensions within 24 h of incubation allowed for the study of endothelialization on structurally stable scaffolds after a

one-day pre-incubation period, indicating the highest levels of cell proliferation observed on SG-3 and SG-4 with the groove width of 9.33 and 22.27 μm , respectively. Moreover, endothelial cells on SG-3 and SG-4 exhibited organized actin filaments aligned with the grooves, with significant elongation and alignment, highlighting the benefits of these topographies. However, slight nuclear deformation on SG-3 suggests a potential risk of dysfunction. While both substrates formed confluent VE-cadherin-positive junctions, SG-4 showed significantly higher vinculin expression, indicating stronger cell attachment. These findings suggest that, particularly SG-4 may offer a more promising surface topography for improved endothelialization compared to other surface topography designs possibly enhancing rapid endothelialization, tissue regeneration and suppressing undesired pro-inflammatory reactions for future *in vitro* and *in vivo* applications.

Acknowledgments

We would like to warmly thank the Institute of Applied Optics (ITO), University of Stuttgart, Germany for providing us with the infrastructure to perform confocal microscopy. The authors thank J. Hohmann and S. Hengsbach for the master fabrication by lithography, S. Bergdolt for electroplating the mold insert, and M. Schneider for the replication in polymer by hot embossing. For language refinement only, some parts of this manuscript were improved using ChatGPT-4.0 (OpenAI). The tool was used solely to enhance clarity and expression in English under full human oversight. All content remains the original work of the authors.

Disclosure statement

No potential conflict of interest was reported by the author(s).

Funding

This work was partly carried out with the support of the Karlsruhe Nano Micro Facility (KNMF, www.knmf.kit.edu) within the project [2021-026-030551].

ORCID

Ali Salehi  <http://orcid.org/0000-0002-2873-6832>

Lena Rutz  <http://orcid.org/0009-0007-9642-4148>

Johanna Stevens  <http://orcid.org/0009-0000-5520-6733>

Markus Guttman  <http://orcid.org/0000-0003-3408-7258>

Giorgio Cattaneo  <http://orcid.org/0000-0003-0550-7049>

References

- [1] Celermajer DS, Chow CK, Marijon E, et al. Cardiovascular disease in the developing world. *J Am Coll Cardiol.* 2012;60(14):1207–1216. doi: [10.1016/j.jacc.2012.03.074](https://doi.org/10.1016/j.jacc.2012.03.074).
- [2] Zhu Z, Ma L, Wu J, et al. A highly realistic hydrogel-based simulated vascular model for surgical hemostasis training. *Compos Commun.* 2025;54:102275. doi: [10.1016/j.coco.2025.102275](https://doi.org/10.1016/j.coco.2025.102275).

- [3] McUsic AC, Lamba DA, Reh TA. Guiding the morphogenesis of dissociated newborn mouse retinal cells and hES cell-derived retinal cells by soft lithography-patterned microchannel PLGA scaffolds. *Biomaterials*. 2012;33(5):1396–1405. doi: [10.1016/j.biomaterials.2011.10.083](https://doi.org/10.1016/j.biomaterials.2011.10.083).
- [4] Zimoch J, Padial JS, Klar AS, et al. Polyisocyanopeptide hydrogels: a novel thermo-responsive hydrogel supporting pre-vascularization and the development of organotypic structures. *Acta Biomater*. 2018;70:129–139. doi: [10.1016/j.actbio.2018.01.042](https://doi.org/10.1016/j.actbio.2018.01.042).
- [5] Chiu YC, Cheng MH, Engel H, et al. The role of pore size on vascularization and tissue remodeling in PEG hydrogels. *Biomaterials*. 2011;32(26):6045–6051. doi: [10.1016/j.biomaterials.2011.04.066](https://doi.org/10.1016/j.biomaterials.2011.04.066).
- [6] Echave MC, Burgo LS, Pedraz JL, et al. Gelatin as biomaterial for tissue engineering. *Curr Pharm Des*. 2017;23(24):3567–3584. doi: [10.2174/0929867324666170511123101](https://doi.org/10.2174/0929867324666170511123101).
- [7] Toborek M, Kaiser S. Endothelial cell functions. Relationship to atherogenesis. *Basic Res Cardiol*. 1999;94(5):295–314. doi: [10.1007/s003950050156](https://doi.org/10.1007/s003950050156).
- [8] Eyckmans J, Boudou T, Yu X, et al. A Hitchhiker's guide to mechanobiology. *Dev Cell*. 2011;21(1):35–47. doi: [10.1016/j.devcel.2011.06.015](https://doi.org/10.1016/j.devcel.2011.06.015).
- [9] Lukashev ME, Werb Z. ECM signalling: orchestrating cell behaviour and misbehaviour. *Trends Cell Biol*. 1998;8(11):437–441. doi: [10.1016/s0962-8924\(98\)01362-2](https://doi.org/10.1016/s0962-8924(98)01362-2).
- [10] Rørth P. Whence directionality: guidance mechanisms in solitary and collective cell migration. *Dev Cell*. 2011;20(1):9–18. doi: [10.1016/j.devcel.2010.12.014](https://doi.org/10.1016/j.devcel.2010.12.014).
- [11] Hynes RO. The extracellular matrix: not just pretty fibrils. *Science*. 2009;326(5957):1216–1219. doi: [10.1126/science.1176009](https://doi.org/10.1126/science.1176009).
- [12] Abrams GA, Goodman SL, Nealey PF, et al. Nanoscale topography of the basement membrane underlying the corneal epithelium of the rhesus macaque. *Cell Tissue Res*. 2000;299(1):39–46. doi: [10.1007/s004410050004](https://doi.org/10.1007/s004410050004).
- [13] Li Y, Huang G, Zhang X, et al. Engineering cell alignment in vitro. *Biotechnol Adv*. 2014;32(2):347–365. doi: [10.1016/j.biotechadv.2013.11.007](https://doi.org/10.1016/j.biotechadv.2013.11.007).
- [14] Salehi A, Sprejz S, Ruehl H, et al. An imprint-based approach to replicate nano- to microscale roughness on gelatin hydrogel scaffolds: surface characterization and effect on endothelialization. *J Biomater Sci Polym Ed*. 2024;35(8):1214–1235.
- [15] Li S, Bhatia S, Hu YL, et al. Effects of morphological patterning on endothelial cell migration. *Biorheology*. 2001;38(2–3):101–108. doi: [10.1177/0006355X2001038002003012](https://doi.org/10.1177/0006355X2001038002003012).
- [16] Biela SA, Su Y, Spatz JP, et al. Different sensitivity of human endothelial cells, smooth muscle cells and fibroblasts to topography in the nano–micro range. *Acta Biomater*. 2009;5(7):2460–2466. doi: [10.1016/j.actbio.2009.04.003](https://doi.org/10.1016/j.actbio.2009.04.003).
- [17] Craighead HG, James CD, Turner AMP. Chemical and topographical patterning for directed cell attachment. *Curr Opin Solid State Mater Sci*. 2001;5(2–3):177–184. doi: [10.1016/S1359-0286\(01\)00005-5](https://doi.org/10.1016/S1359-0286(01)00005-5).
- [18] Jung DR, Kapur R, Adams T, et al. Topographical and physicochemical modification of material surface to enable patterning of living cells. *Crit Rev Biotechnol*. 2001;21(2):111–154. doi: [10.1080/20013891081700](https://doi.org/10.1080/20013891081700).
- [19] Potthoff E, Franco D, D'Alessandro V, et al. Toward a rational design of surface textures promoting endothelialization. *Nano Lett*. 2014;14(2):1069–1079. doi: [10.1021/nl4047398](https://doi.org/10.1021/nl4047398).
- [20] DuFort CC, Paszek MJ, Weaver VM. Balancing forces: architectural control of mechanotransduction. *Nat Rev Mol Cell Biol*. 2011;12(5):308–319. doi: [10.1038/nrm3112](https://doi.org/10.1038/nrm3112).
- [21] Salehi A, Mobarhan MA, Mohammadi J, et al. Natural cellulose-based scaffold for improvement of stem cell osteogenic differentiation. *J Drug Deliv Sci Technol*. 2021;63:102453.
- [22] Woo KM, Chen VJ, Ma PX. Nano-fibrous scaffolding architecture selectively enhances protein adsorption contributing to cell attachment. *J Biomed Mater Res A*. 2003;67(2):531–537. doi: [10.1002/jbm.a.10098](https://doi.org/10.1002/jbm.a.10098).
- [23] Zhuang Y, Zhang C, Cheng M, et al. Challenges and strategies for in situ endothelialization and long-term lumen patency of vascular grafts. *Bioact Mater*. 2021;6(6):1791–1809. doi: [10.1016/j.bioactmat.2020.11.028](https://doi.org/10.1016/j.bioactmat.2020.11.028).

- [24] Kakinoki S, Takasaki K, Mahara A, et al. Direct surface modification of metallic bio-materials via tyrosine oxidation aiming to accelerate the re-endothelialization of vascular stents. *J Biomed Mater Res A*. 2018;106(2):491–499. doi: [10.1002/jbm.a.36258](https://doi.org/10.1002/jbm.a.36258).
- [25] Lemmens TP, Bröker V, Rijpkema M, et al. Fundamental considerations for designing endothelialized in vitro models of thrombosis. *Thromb Res*. 2024;236:179–190. doi: [10.1016/j.thromres.2024.03.004](https://doi.org/10.1016/j.thromres.2024.03.004).
- [26] Friedl P, Sahai E, Weiss S, et al. New dimensions in cell migration. *Nat Rev Mol Cell Biol*. 2012;13(11):743–747. doi: [10.1038/nrm3459](https://doi.org/10.1038/nrm3459).
- [27] Vartanian KB, Kirkpatrick SJ, Hanson SR, et al. Endothelial cell cytoskeletal alignment independent of fluid shear stress on micropatterned surfaces. *Biochem Biophys Res Commun*. 2008;371(4):787–792. doi: [10.1016/j.bbrc.2008.04.167](https://doi.org/10.1016/j.bbrc.2008.04.167).
- [28] Aubin H, Nichol JW, Hutson CB, et al. Directed 3D cell alignment and elongation in microengineered hydrogels. *Biomaterials*. 2010;31(27):6941–6951. doi: [10.1016/j.biomaterials.2010.05.056](https://doi.org/10.1016/j.biomaterials.2010.05.056).
- [29] Tsai IY, Crosby AJ, Russell TP. Surface patterning. *Methods Cell Biol*. 2007;83:67–87. doi: [10.1016/S0091-679X\(07\)83004-4](https://doi.org/10.1016/S0091-679X(07)83004-4).
- [30] Curtis A, Wilkinson C. Topographical control of cells. *Biomaterials*. 1997;18(24):1573–1583. doi: [10.1016/s0142-9612\(97\)00144-0](https://doi.org/10.1016/s0142-9612(97)00144-0).
- [31] Tenje M, Cantoni F, Porras Hernández AM, et al. A practical guide to microfabrication and patterning of hydrogels for biomimetic cell culture scaffolds. *Organs-on-a-Chip*. 2020;2:100003. doi: [10.1016/j.ooc.2020.100003](https://doi.org/10.1016/j.ooc.2020.100003).
- [32] Buck R. Behaviour of vascular smooth muscle cells during repeated stretching of the substratum in vitro. *Atherosclerosis*. 1983;46(2):217–223. doi: [10.1016/0021-9150\(83\)90112-0](https://doi.org/10.1016/0021-9150(83)90112-0).
- [33] Walboomers XF, Croes HJE, Ginsel LA, et al. Contact guidance of rat fibroblasts on various implant materials. *J Biomed Mater Res*. 1999;47(2):204–212. doi: [10.1002/\(SICI\)1097-4636\(199911\)47:2<204::AID-JBM10>3.0.CO;2-H](https://doi.org/10.1002/(SICI)1097-4636(199911)47:2<204::AID-JBM10>3.0.CO;2-H).
- [34] Brunette DM, Chehroudi B. The effects of the surface topography of micromachined titanium substrata on cell behavior in vitro and in vivo. *J Biomech Eng*. 1999;121(1):49–57. doi: [10.1115/1.2798042](https://doi.org/10.1115/1.2798042).
- [35] Yung CW, Wu LQ, Tullman JA, et al. Transglutaminase crosslinked gelatin as a tissue engineering scaffold. *J Biomed Mater Res A*. 2007;83A(4):1039–1046. doi: [10.1002/jbm.a.31431](https://doi.org/10.1002/jbm.a.31431).
- [36] Yang G, Xiao Z, Ren X, et al. Enzymatically crosslinked gelatin hydrogel promotes the proliferation of adipose tissue-derived stromal cells. *PeerJ*. 2016;4:e2497. doi: [10.7717/peerj.2497](https://doi.org/10.7717/peerj.2497).
- [37] Hu X, Ma L, Wang C, et al. Gelatin hydrogel prepared by photo-initiated polymerization and loaded with TGF- β 1 for cartilage tissue engineering. *Macromol Biosci*. 2009;9(12):1194–1201. doi: [10.1002/mabi.200900275](https://doi.org/10.1002/mabi.200900275).
- [38] Moreira Teixeira LS, Feijen J, van Blitterswijk CA, et al. Enzyme-catalyzed crosslinkable hydrogels: emerging strategies for tissue engineering. *Biomaterials*. 2012;33(5):1281–1290. doi: [10.1016/j.biomaterials.2011.10.067](https://doi.org/10.1016/j.biomaterials.2011.10.067).
- [39] Dell’Olmo E, Gaglione R, Arciello A, et al. Transglutaminase-mediated crosslinking of a host defence peptide derived from human apolipoprotein B and its effect on the peptide antimicrobial activity. *Biochim Biophys Acta Gen Subj*. 2021;1865(2):129803. doi: [10.1016/j.bbagen.2020.129803](https://doi.org/10.1016/j.bbagen.2020.129803).
- [40] Mostafa HS. Microbial transglutaminase: an overview of recent applications in food and packaging. *Biocatal Biotransformation*. 2020;38(3):161–177. doi: [10.1080/10242422.2020.1720660](https://doi.org/10.1080/10242422.2020.1720660).
- [41] Chen T, Embree HD, Brown EM, et al. Enzyme-catalyzed gel formation of gelatin and chitosan: potential for in situ applications. *Biomaterials*. 2003;24(17):2831–2841. doi: [10.1016/s0142-9612\(03\)00096-6](https://doi.org/10.1016/s0142-9612(03)00096-6).
- [42] Luo Y, Chen B, Zhang X, et al. 3D printed concentrated alginate/GelMA hollow-fibers-packed scaffolds with nano apatite coatings for bone tissue engineering. *Int J Biol Macromol*. 2022;202:366–374. doi: [10.1016/j.ijbiomac.2022.01.096](https://doi.org/10.1016/j.ijbiomac.2022.01.096).

- [43] Chen C, Tang J, Gu Y, et al. Bioinspired hydrogel electrospun fibers for spinal cord regeneration. *Adv Funct Mater.* 2019;29(4):1806899.
- [44] Leclech C, Barakat AI. Is there a universal mechanism of cell alignment in response to substrate topography? *Cytoskeleton.* 2021;78(6):284–292. doi: [10.1002/cm.21661](https://doi.org/10.1002/cm.21661).
- [45] McDermott MK, Chen T, Williams CM, et al. Mechanical properties of biomimetic tissue adhesive based on the microbial transglutaminase-catalyzed crosslinking of gelatin. *Biomacromolecules.* 2004;5(4):1270–1279. doi: [10.1021/bm034529a](https://doi.org/10.1021/bm034529a).
- [46] Shi X, Ostrovidov S, Zhao Y, et al. Microfluidic spinning of cell-responsive grooved microfibers. *Adv Funct Materials.* 2015;25(15):2250–2259. doi: [10.1002/adfm.201404531](https://doi.org/10.1002/adfm.201404531).
- [47] Blume C, Kraus X, Heene S, et al. Vascular implants – new aspects for in situ tissue engineering. *Eng Life Sci.* 2022;22(3-4):344–360. doi: [10.1002/elsc.202100100](https://doi.org/10.1002/elsc.202100100).
- [48] Gan D, Xu T, Xing W, et al. Mussel-inspired dopamine oligomer intercalated tough and resilient gelatin methacryloyl (GelMA) hydrogels for cartilage regeneration. *J Mater Chem B.* 2019;7(10):1716–1725. doi: [10.1039/c8tb01664j](https://doi.org/10.1039/c8tb01664j).
- [49] Han L, Xu J, Lu X, et al. Biohybrid methacrylated gelatin/polyacrylamide hydrogels for cartilage repair. *J Mater Chem B.* 2017;5(4):731–741. doi: [10.1039/c6tb02348g](https://doi.org/10.1039/c6tb02348g).
- [50] Salehi A, Mobarhan MA, Mohammadi J, et al. Cabbage-derived three-dimensional cellulose scaffold-induced osteogenic differentiation of stem cells. *J Cell Physiol.* 2021;236(7):5306–5316. doi: [10.1002/jcp.30239](https://doi.org/10.1002/jcp.30239).
- [51] Sprague EA, Tio F, Ahmed SH, et al. Impact of parallel micro-engineered stent grooves on endothelial cell migration, proliferation, and function. *Circ Cardiovasc Interv.* 2012;5(4):499–507. doi: [10.1161/CIRCINTERVENTIONS.111.967901](https://doi.org/10.1161/CIRCINTERVENTIONS.111.967901).
- [52] Rajendran P, Rengarajan T, Thangavel J, et al. The vascular endothelium and human diseases. *Int J Biol Sci.* 2013;9(10):1057–1069. doi: [10.7150/ijbs.7502](https://doi.org/10.7150/ijbs.7502).
- [53] Stowell CET, Wang Y. Quickening: translational design of resorbable synthetic vascular grafts. *Biomaterials.* 2018;173:71–86. doi: [10.1016/j.biomaterials.2018.05.006](https://doi.org/10.1016/j.biomaterials.2018.05.006).
- [54] Yi B, Zhou B, Song Z, et al. Step-wise CAG@PLys@PDA-Cu²⁺ modification on micro-patterned nanofibers for programmed endothelial healing. *Bioact Mater.* 2023;25:657–676. doi: [10.1016/j.bioactmat.2022.07.010](https://doi.org/10.1016/j.bioactmat.2022.07.010).
- [55] Kimura T, Kondo M, Hashimoto Y, et al. Surface topography of PDMS replica transferred from various decellularized aortic lumens affects cellular orientation. *ACS Biomater Sci Eng.* 2019;5(11):5721–5726. doi: [10.1021/acsbiomaterials.8b01536](https://doi.org/10.1021/acsbiomaterials.8b01536).
- [56] Thomsen MS, Routhe LJ, Moos T. The vascular basement membrane in the healthy and pathological brain. *J Cereb Blood Flow Metab.* 2017;37(10):3300–3317. doi: [10.1177/0271678X17722436](https://doi.org/10.1177/0271678X17722436).
- [57] Conner AA, David D, Yim EKF. The effects of biomimetic surface topography on vascular cells: implications for vascular conduits. *Adv Healthc Mater.* 2024;13(27):e2400335. doi: [10.1002/adhm.202400335](https://doi.org/10.1002/adhm.202400335).
- [58] Skopinska-Wisniewska J, Tuszyńska M, Olewnik-Kruszkowska E. Comparative study of gelatin hydrogels modified by various cross-linking agents. *Materials.* 2021;14(2):396. doi: [10.3390/ma14020396](https://doi.org/10.3390/ma14020396).
- [59] Luo X, Liu Y, Pang J, et al. Thermo/photo dual-crosslinking chitosan-gelatin methacrylate hydrogel with controlled shrinking property for contraction fabrication. *Carbohydr Polym.* 2020;236:116067. doi: [10.1016/j.carbpol.2020.116067](https://doi.org/10.1016/j.carbpol.2020.116067).
- [60] Vlierberghe SV, Schacht E, Dubrue P. Reversible gelatin-based hydrogels: finetuning of material properties. *Eur Polym J.* 2011;47(5):1039–1047. doi: [10.1016/j.eurpolymj.2011.02.015](https://doi.org/10.1016/j.eurpolymj.2011.02.015).
- [61] Song Y, Wehmeyer G. Maximizing and minimizing the boundary scattering mean free path in diameter-modulated coaxial cylindrical nanowires. *J Appl Phys.* 2021;130(4):045104.
- [62] Carvalho IC, Mansur HS. Engineered 3D-scaffolds of photocrosslinked chitosan-gelatin hydrogel hybrids for chronic wound dressings and regeneration. *Mater Sci Eng C Mater Biol Appl.* 2017;78:690–705. doi: [10.1016/j.msec.2017.04.126](https://doi.org/10.1016/j.msec.2017.04.126).

- [63] Wisotzki EI, Hennes M, Schuldt C, et al. Tailoring the material properties of gelatin hydrogels by high energy electron irradiation. *J Mater Chem B*. 2014;2(27):4297–4309. doi: [10.1039/c4tb00429a](https://doi.org/10.1039/c4tb00429a).
- [64] Tadsen M, Friedrich RP, Riedel S, et al. Contact guidance by microstructured gelatin hydrogels for prospective tissue engineering applications. *ACS Appl Mater Interfaces*. 2019;11(7):7450–7458. doi: [10.1021/acsami.8b21638](https://doi.org/10.1021/acsami.8b21638).
- [65] Tielrooij KJ, Garcia-Araez N, Bonn M, et al. Cooperativity in ion hydration. *Science*. 2010;328(5981):1006–1009. doi: [10.1126/science.1183512](https://doi.org/10.1126/science.1183512).
- [66] Ohba T, Hata K, Kanoh H. Significant hydration shell formation instead of hydrogen bonds in nanoconfined aqueous electrolyte solutions. *J Am Chem Soc*. 2012;134(43):17850–17853. doi: [10.1021/ja307338t](https://doi.org/10.1021/ja307338t).
- [67] English AE, Tanaka T, Edelman ER. Polymer and solution ion shielding in polyampholytic hydrogels. *Polymer*. 1998;39(24):5893–5897. doi: [10.1016/S0032-3861\(98\)00106-2](https://doi.org/10.1016/S0032-3861(98)00106-2).
- [68] Leiendecker M, Licht CJ, Borghs J, et al. Physical polyurethane hydrogels via charge shielding through acids or salts. *Macromol Rapid Commun*. 2018;39(7):e1700711. doi: [10.1002/marc.201700711](https://doi.org/10.1002/marc.201700711).
- [69] Ostroha J, Pong M, Lowman A, et al. Controlling the collapse/swelling transition in charged hydrogels. *Biomaterials*. 2004;25(18):4345–4353. doi: [10.1016/j.biomaterials.2003.11.019](https://doi.org/10.1016/j.biomaterials.2003.11.019).
- [70] Jepsen ML, Nielsen LH, Boisen A, et al. Characterization of thin gelatin hydrogel membranes with balloon properties for dynamic tissue engineering. *Biopolymers*. 2019;110(1):e23241. doi: [10.1002/bip.23241](https://doi.org/10.1002/bip.23241).
- [71] Khorshidi S, Karkhaneh A. A self-crosslinking tri-component hydrogel based on functionalized polysaccharides and gelatin for tissue engineering applications. *Mater Lett*. 2016;164:468–471. doi: [10.1016/j.matlet.2015.11.041](https://doi.org/10.1016/j.matlet.2015.11.041).
- [72] VanBavel E, Siersma P, Spaan JAE. Elasticity of passive blood vessels: a new concept. *Am J Physiol Heart Circ Physiol*. 2003;285(5):H1986–2000. doi: [10.1152/ajpheart.00248.2003](https://doi.org/10.1152/ajpheart.00248.2003).
- [73] Silver FH. In vivo non-invasive analysis of the mechanical properties of vessel walls using vibrational optical coherence tomography. *OJCRR*. 2021;5(1). doi: [10.33552/OJCRR.2021.05.000603](https://doi.org/10.33552/OJCRR.2021.05.000603).
- [74] Cheng J, Wang C, Gu Y. Combination of freeze-thaw with detergents: a promising approach to the decellularization of porcine carotid arteries. *Biomed Mater Eng*. 2019;30(2):191–205. doi: [10.3233/BME-191044](https://doi.org/10.3233/BME-191044).
- [75] Yokota Y, Kawamura Y, Nogata F, et al. Carotid elastic modulus in vivo estimation using ultrasonic images and comparison to in vitro measurement for animal. Paper presented at: World Congress on Medical Physics and Biomedical Engineering, September 7–12, 2009, Munich, Germany, 2009. p. 1226–1229.
- [76] Rk V, Joseph PMN, Shah J, et al. Measurement of arterial Young's elastic modulus using ARTSENS pen. Paper presented at: 2018 IEEE International Symposium on Medical Measurements and Applications (MeMeA). IEEE; 2018. p. 1–6.
- [77] Matsuda T, Nakayama Y. Surface microarchitectural design in biomedical applications: in vitro transmural endothelialization on microporous segmented polyurethane films fabricated using an excimer laser. *J Biomed Mater Res*. 1996;31(2):235–242. doi: [10.1002/\(SICI\)1097-4636\(199606\)31:2<235::AID-JBM10>3.0.CO;2-K](https://doi.org/10.1002/(SICI)1097-4636(199606)31:2<235::AID-JBM10>3.0.CO;2-K).
- [78] Lei Y, Zouani OF, Rémy M, et al. Geometrical microfeature cues for directing tubulogenesis of endothelial cells. *PLoS One*. 2012;7(7):e41163. doi: [10.1371/journal.pone.0041163](https://doi.org/10.1371/journal.pone.0041163).
- [79] Chen JY, Hu M, Zhang H, et al. Improved antithrombotic function of oriented endothelial cell monolayer on microgrooves. *ACS Biomater Sci Eng*. 2018;4(6):1976–1985.
- [80] Franco D, Klingauf M, Bednarzik M, et al. Control of initial endothelial spreading by topographic activation of focal adhesion kinase. *Soft Matter*. 2011;7(16):7313. doi: [10.1039/c1sm05191a](https://doi.org/10.1039/c1sm05191a).
- [81] Uttayarat P, Toworfe GK, Dietrich F, et al. Topographic guidance of endothelial cells on silicone surfaces with micro- to nanogrooves: orientation of actin filaments and focal adhesions. *J Biomed Mater Res A*. 2005;75A(3):668–680. doi: [10.1002/jbm.a.30478](https://doi.org/10.1002/jbm.a.30478).

- [82] Charest JL, Eliason MT, García AJ, et al. Polymer cell culture substrates with combined nanotopographical patterns and micropatterned chemical domains. *J Vac Sci Technol B*. 2005;23(6):3011–3014. doi: [10.1116/1.2127951](https://doi.org/10.1116/1.2127951).
- [83] Chen CS, Mrksich M, Huang S, et al. Geometric control of cell life and death. *Science*. 1997;276(5317):1425–1428. doi: [10.1126/science.276.5317.1425](https://doi.org/10.1126/science.276.5317.1425).
- [84] Chen T-G, Chen JZ, Wang X-X. Effects of rapamycin on number activity and eNOS of endothelial progenitor cells from peripheral blood. *Cell Prolif*. 2006;39(2):117–125. doi: [10.1111/j.1365-2184.2006.00375.x](https://doi.org/10.1111/j.1365-2184.2006.00375.x).
- [85] Chen CS, Mrksich M, Huang S, et al. Micropatterned surfaces for control of cell shape, position, and function. *Biotechnol Prog*. 1998;14(3):356–363. doi: [10.1021/bp980031m](https://doi.org/10.1021/bp980031m).
- [86] Dike LE, Chen CS, Mrksich M, et al. Geometric control of switching between growth, apoptosis, and differentiation during angiogenesis using micropatterned substrates. *In Vitro Cell Dev Biol Anim*. 1999;35(8):441–448. doi: [10.1007/s11626-999-0050-4](https://doi.org/10.1007/s11626-999-0050-4).
- [87] Kato S, Ando J, Matsuda T. mRNA expression on shape-engineered endothelial cells: adhesion molecules ICAM-1 and VCAM-1. *J Biomed Mater Res*. 2001;54(3):366–372. doi: [10.1002/1097-4636\(20010305\)54:3<366::AID-JBM80>3.0.CO;2-R](https://doi.org/10.1002/1097-4636(20010305)54:3<366::AID-JBM80>3.0.CO;2-R).
- [88] Leclech C, Roellinger B, Frederick J, et al. Microgroove substrates unveil topography-driven, dynamic 3D nuclear deformations. 2024. <https://www.biorxiv.org/content/10.1101/2024.02.02.578638v1>
- [89] Roca-Cusachs P, Alcaraz J, Sunyer R, et al. Micropatterning of single endothelial cell shape reveals a tight coupling between nuclear volume in G1 and proliferation. *Biophys J*. 2008;94(12):4984–4995. doi: [10.1529/biophysj.107.116863](https://doi.org/10.1529/biophysj.107.116863).
- [90] McKee CT, Raghunathan VK, Nealey PF, et al. Topographic modulation of the orientation and shape of cell nuclei and their influence on the measured elastic modulus of epithelial cells. *Biophys J*. 2011;101(9):2139–2146. doi: [10.1016/j.bpj.2011.09.042](https://doi.org/10.1016/j.bpj.2011.09.042).
- [91] Malek AM, Izumo S. Mechanism of endothelial cell shape change and cytoskeletal remodeling in response to fluid shear stress. *J Cell Sci*. 1996;109 (Pt 4)(4):713–726. doi: [10.1242/jcs.109.4.713](https://doi.org/10.1242/jcs.109.4.713).
- [92] Gamboa JR, Mohandes S, Tran PL, et al. Linear fibroblast alignment on sinusoidal wave micro-patterns. *Colloids Surf B Biointerfaces*. 2013;104:318–325. doi: [10.1016/j.colsurfb.2012.11.035](https://doi.org/10.1016/j.colsurfb.2012.11.035).
- [93] Jaffe EA. Cell biology of endothelial cells. *Hum Pathol*. 1987;18(3):234–239. doi: [10.1016/s0046-8177\(87\)80005-9](https://doi.org/10.1016/s0046-8177(87)80005-9).
- [94] Natale CF, Lafaurie-Janvore J, Ventre M, et al. Focal adhesion clustering drives endothelial cell morphology on patterned surfaces. *J R Soc Interface*. 2019;16(158):20190263. doi: [10.1098/rsif.2019.0263](https://doi.org/10.1098/rsif.2019.0263).
- [95] Jiang X, Takayama S, Qian X, et al. Controlling mammalian cell spreading and cytoskeletal arrangement with conveniently fabricated continuous wavy features on poly(dimethylsiloxane). *Langmuir*. 2002;18(8):3273–3280.
- [96] Sun B, Xie K, Chen TH, et al. Preferred cell alignment along concave microgrooves. *RSC Adv*. 2017;7(11):6788–6794. doi: [10.1039/C6RA26545F](https://doi.org/10.1039/C6RA26545F).
- [97] Nerem RM, Levesque MJ, Cornhill JF. Vascular endothelial morphology as an indicator of the pattern of blood flow. *J Biomech Eng*. 1981;103(3):172–176. doi: [10.1115/1.3138275](https://doi.org/10.1115/1.3138275).
- [98] Lu J, Rao MP, MacDonald NC, et al. Improved endothelial cell adhesion and proliferation on patterned titanium surfaces with rationally designed, micrometer to nanometer features. *Acta Biomater*. 2008;4(1):192–201. doi: [10.1016/j.actbio.2007.07.008](https://doi.org/10.1016/j.actbio.2007.07.008).
- [99] Ma W, Liu L, Luo X, et al. Effects of biomimetic micropattern on titanium deposited with PDA/Cu and nitric oxide release on behaviors of ECs. *J Mater Res*. 2019;34(12):2037–2046. doi: [10.1557/jmr.2019.166](https://doi.org/10.1557/jmr.2019.166).
- [100] Ma W, Liu L, Chen H, et al. Micropatterned immobilization of membrane-mimicking polymer and peptides for regulation of cell behaviors *in vitro*. *RSC Adv*. 2018;8(37):20836–20850. doi: [10.1039/c8ra02607f](https://doi.org/10.1039/c8ra02607f).
- [101] Govindarajan T, Shandas R. Microgrooves encourage endothelial cell adhesion and organization on shape-memory polymer surfaces. *ACS Appl Bio Mater*. 2019;2(5):1897–1906. doi: [10.1021/acsabm.8b00833](https://doi.org/10.1021/acsabm.8b00833).

- [102] Zebda N, Dubrovskiy O, Birukov KG. Focal adhesion kinase regulation of mechano-transduction and its impact on endothelial cell functions. *Microvasc Res.* 2012;83(1):71–81. doi: [10.1016/j.mvr.2011.06.007](https://doi.org/10.1016/j.mvr.2011.06.007).
- [103] Salehi A, Ernez M, Salido GL, et al. Toward “green” vessels: characterization of micro-structure, mechanics, and endothelial cell interaction on three macro-tubular plants for vascular tissue engineering applications. *Adv Mater Technol.* 2024;10(7):2401129.
- [104] Kooten TGV, Recum AFV. Cell adhesion to textured silicone surfaces: the influence of time of adhesion and texture on focal contact and fibronectin fibril formation. *Tissue Eng.* 1999;5(3):223–240. doi: [10.1089/ten.1999.5.223](https://doi.org/10.1089/ten.1999.5.223).
- [105] den Braber ET, de Ruijter JE, Ginsel LA, et al. Orientation of ECM protein deposition, fibroblast cytoskeleton, and attachment complex components on silicone microgrooved surfaces. *J Biomed Mater Res.* 1998;40(2):291–300. doi: [10.1002/\(SICI\)1097-4636\(199805\)40:2<291::AID-JBM14>3.3.CO;2-8](https://doi.org/10.1002/(SICI)1097-4636(199805)40:2<291::AID-JBM14>3.3.CO;2-8).
- [106] Dejana E, Vestweber D. The role of VE-cadherin in vascular morphogenesis and permeability control. *Prog Mol Biol Transl Sci.* 2013;116:119–144. doi: [10.1016/B978-0-12-394311-8.00006-6](https://doi.org/10.1016/B978-0-12-394311-8.00006-6).
- [107] Fernández-Castillejo S, Formentín P, Catalán Ú, et al. Silicon microgrooves for contact guidance of human aortic endothelial cells. *Beilstein J Nanotechnol.* 2017;8:675–681. doi: [10.3762/bjnano.8.72](https://doi.org/10.3762/bjnano.8.72).
- [108] Wu CC, Li YS, Haga JH, et al. Directional shear flow and Rho activation prevent the endothelial cell apoptosis induced by micropatterned anisotropic geometry. *Proc Natl Acad Sci U S A.* 2007;104(4):1254–1259. doi: [10.1073/pnas.0609806104](https://doi.org/10.1073/pnas.0609806104).
- [109] Liang J, Gu S, Mao X, et al. Endothelial cell morphology regulates inflammatory cells through microRNA transferred by extracellular vesicles. *Front Bioeng Biotechnol.* 2020;8:369. doi: [10.3389/fbioe.2020.00369](https://doi.org/10.3389/fbioe.2020.00369).
- [110] Indolfi L, Baker AB, Edelman ER. The role of scaffold microarchitecture in engineering endothelial cell immunomodulation. *Biomaterials.* 2012;33(29):7019–7027. doi: [10.1016/j.biomaterials.2012.06.052](https://doi.org/10.1016/j.biomaterials.2012.06.052).
- [111] Jeon J, An S, Bae J, et al. Development of microbial transglutaminase-crosslinked gelatin hydrogel gratings with structural stability under high-stretching conditions for induction of muscle hypertrophy. *J Ind Eng Chem.* 2023;124:348–357. doi: [10.1016/j.jiec.2023.04.029](https://doi.org/10.1016/j.jiec.2023.04.029).
- [112] Yi B, Xu Q, Liu W. An overview of substrate stiffness guided cellular response and its applications in tissue regeneration. *Bioact Mater.* 2022;15:82–102. doi: [10.1016/j.bioact-mat.2021.12.005](https://doi.org/10.1016/j.bioact-mat.2021.12.005).